sets (corresponding to ~33,000 human genes) were then determined for Blast Bank specimens derived from 83 individuals with AML and 16 individuals in the advanced stage [refractory anemia with excess of blasts (RAEB)] of MDS. The clinical characteristics of the study subjects are provided in Table I.

For analysis of the expression data, the criterion that the expression level of a given probe set should receive the "Present" call (from Microarray Suite 5.0 software) in at least 30% (n=30) of the samples was applied in order to exclude transcriptionally-silent genes from the analysis. A total of 11,595 probe sets passed this selection window. Unsupervised two-way hierarchical clustering analysis (17) was then applied to the 99 patients based on the expression profiles of these 11,595 probe sets, generating a dendrogram of the subjects (Figure 1B). Six out of the 16 patients with RAEB (MDS) clustered together in the dendrogram, whereas the remaining ten RAEB patients were intermixed with the AML cases. Given that eleven of our AML subjects had experienced a previous MDS phase, it was not surprising that the gene expression profiles did not clearly separate RAEB from heterogeneous AML.

Patients with a normal karyotype or "other" abnormalities (<3 or ≥3) were widely distributed throughout the dendrogram, indicative of the highly heterogeneous character of their blasts. Previous unsupervised clustering analysis of the gene expression profiles of BM MNCs from individuals with AML separated the patients into subgroups that were strongly related to the FAB subtype (18, 19). However, such a relationship was not apparent in our analysis of $CD133^+$ cells (data not shown), suggesting that changes in gene expression that accompany the differentiation of leukemic blasts within BM might greatly influence the overall gene expression profiles of MNCs.

Gene expression profiles linked to good prognosis. Among the 83 AML patients studied, 66 individuals were treated with standard chemotherapeutic regimens according to the protocols of the Japan Adult Leukaemia Study Group (JALSG). Kaplan-Meier analysis of these 66 cases revealed that, although the prognosis of individuals with the adverse karyotype was significantly worse than that of the other two karyotype groups (long-rank test, $p<0.001$), the prognosis of patients with the favorable karyotype did not differ from that of those with the intermediate one ($p=0.06$) (Figure 2). The poor prognosis of individuals with the adverse karyotype (5-year survival rate of ~10%) has been confirmed extensively (1, 4, 20), but the intermediate group apparently contains both patients with a curable disorder and those with an intractable one. It is, therefore, of clinical importance to be able to identify individuals with a *bona fide* good prognosis from among those with a favorable or intermediate karyotype.

We next compared the transcriptomes of individuals with these two karyotype designations. Among the 66 AML patients who underwent standard chemotherapy, the blasts of 16 and 39 individuals had the favorable and intermediate karyotypes, respectively. Probe sets that received the "Present" call in ≥10% (n=6) of these 55 cases were selected first. The selected 17,724 probe sets were then screened for those whose expression differed significantly between the two karyotype groups (Student's *t*-test, $p<0.001$), resulting in the identification of 378 such sets. Application of principal component analysis reduced the number of principal gene expression patterns from 378 to three. On the basis of the calculated coordinates of these three principal expression patterns, the 55 samples were projected into a virtual three-dimensional space (Figure 3A). The samples with favorable and intermediate karyotypes were not clearly separated from each other, however.

We, therefore, examined whether it was possible to identify a gene expression profile, or "molecular signature," that was directly linked to the prognosis of leukemic patients. Among the 55 patients with favorable or intermediate karyotypes who underwent standard chemotherapy, 14 individuals survived for ≥755 days (long-term survivors) and eight individuals died within 365 days (short-term survivors) after the first chemotherapy. The application of the Student's *t*-test to the gene expression data for these 22 cases identified five probe sets, the expression level of which contrasted the two groups ($p<0.001$) (Table II). Principal component analysis and three-dimensional projection indicated that the molecular signature was clearly different between the two patient classes (Figure 3B).

Gene expression-based stratification scheme for AML. We next attempted to develop a gene expression-based stratification (GES) system for AML. Given that the adverse karyotype is a reliable indicator of poor prognosis, we tried to construct a GES scheme to isolate those individuals with good prognosis from other patients. The 66 AML patients who underwent standard chemotherapy were divided into training (n=44) and test (n=22) sets (Figure 4A). The former contained 37 patients with favorable or intermediate karyotypes, seven and six of whom were long-term or short-term survivors, respectively. To identify a prognosis-related molecular signature, the Student's *t*-test was first applied to the expression data for these latter 13 cases to isolate probe sets whose expression differed significantly ($p<0.01$) between the two groups. The expression profiles of the resulting 38 probe sets were then subjected to Cox's proportional-hazard regression analysis (21) ($p<0.01$) for the 13 selected individuals. Four independent probe sets (outcome predictor genes) were finally isolated, the expression profiles of which are shown in a dendrogram in Figure 3B. The risk index (RI)

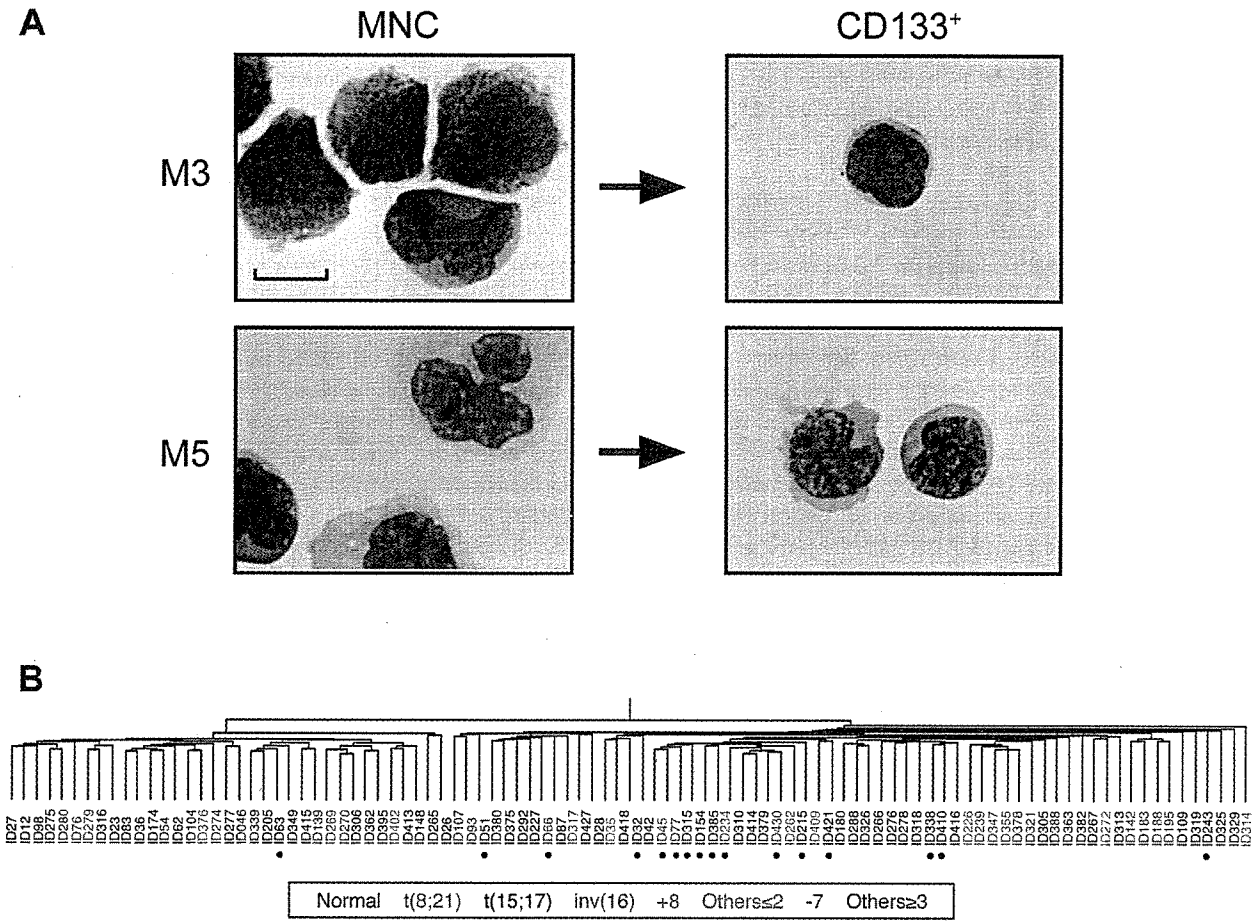

Figure 1. *Clustering analysis of purified CD133+ fractions from individuals with acute myeloid leukemia (AML)-related disorders. A) The CD133+ fractions (right panels) were purified from bone marrow mononuclear cells (MNCs) (left panels) of AML patients of FAB subtypes M3 (upper panels) or M5 (lower panels). The cells were stained with Wright-Giemsa solution. Scale bar, 10 μm. B) Unsupervised clustering of the study subjects based on the similarity in expression profiles of 11,595 probe sets. The karyotype of each patient is colored differentially. Individuals with refractory anemia with excess blasts are indicated by dots.*

(22) was calculated for each patient based on the expression intensity and the parameter estimate (Table III) for each of these four probe sets.

A GES system for AML, based on a combination of this RI-based classification scheme and the karyotype-based scheme, is thus proposed (Figure 5A). AML patients with an adverse karyotype are classified as GES class III, whereas the other patients are classified as either GES class I (RI < –9.36) or GES class II (RI ≥ –9.36) on the basis of the calculated RI for the four outcome predictor genes. To examine whether the GES system is able to select patients with good prognosis, Kaplan-Meier analysis was performed with the 44 individuals in the training set classified according either to the karyotype-based scheme (Figure 5B) or to our GES scheme (Figure 5C). The prognosis of the favorable group of the karyotype-based classification did not

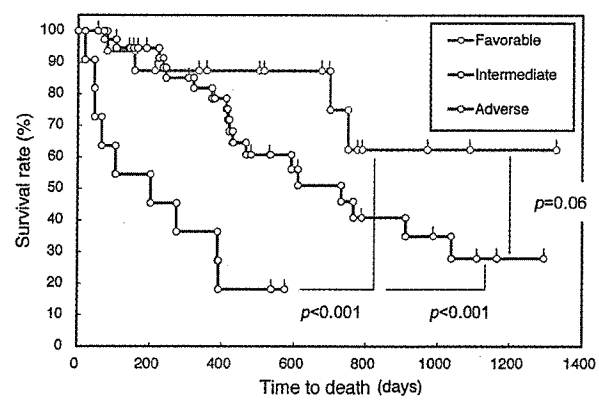

Figure 2. *Long-term survival according to the keryotype-based stratification of the 66 acute myeloid leukemia patients treated with standard chemotherapy.*

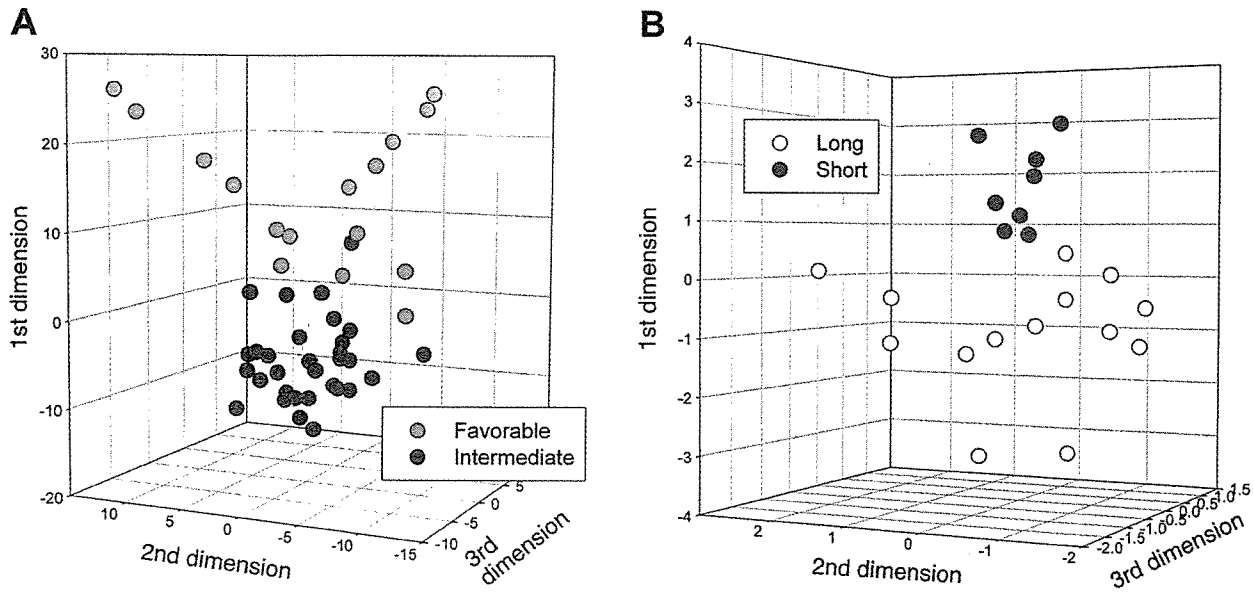

Figure 3. *Comparison of gene expression profiles by principal component analysis. A) Three principal components were derived from the gene expression patterns of 378 probe sets that contrasted acute myeloid leukemia (AML) patients with favorable or intermediate karyotypes who underwent standard chemotherapy. Samples were projected into a virtual space based on the coordinates of the three components. B) Sample projection was similarly performed for five probe sets that contrasted the long-term and short-term survivors among the patients in A.*

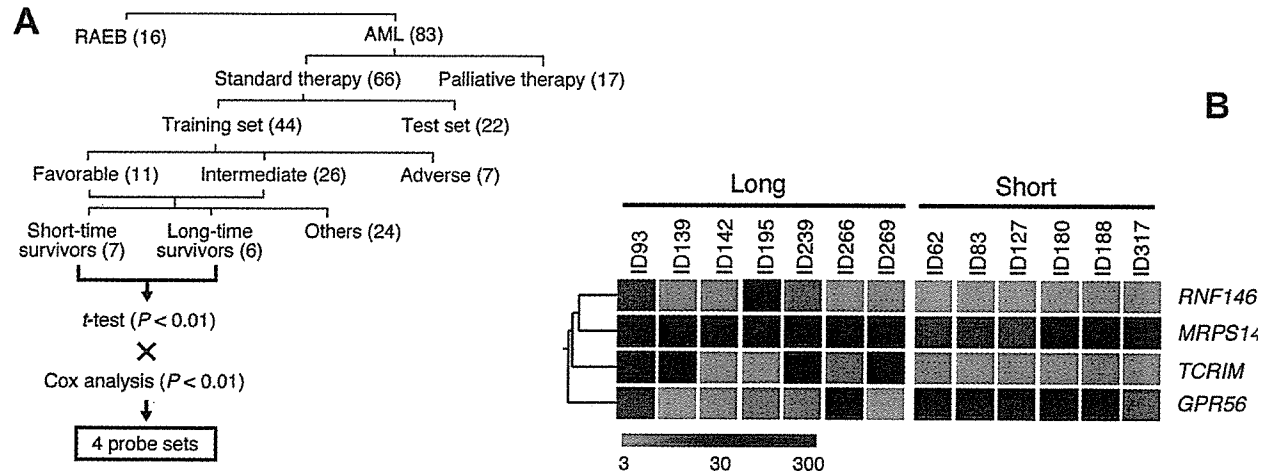

Figure 4. *Isolation of probe sets linked to survival time. A) Approach adopted to identify four probe sets whose expression contrasted the long-term and short-term survivors in a training set of acute myeloid leukemia (AML) patients. The numbers in parentheses indicate the corresponding numbers of subjects. RAEB; refractory anemia with excess of blasts. B) Gene tree for the expression levels (color coded as indicated by the scale at the bottom) of the four human genes identified in A for CD133$^+$ cells derived from seven long-term and six short-term survivors. Each row corresponds to a single gene (symbol shown at right) and each column to a different patient (Blast Bank ID shown at top).*

differ significantly (log-rank test, $p=0.10$) from that of the intermediate group. In contrast, the GES system clearly separated the patients into three groups with distinct prognoses. Importantly, only GES class I contained the long-term survivors.

The efficacy of the GES system was then examined with the 22 individuals in the test set, who were also classified by either the karyotype-based (Figure 5D) or GES (Figure 5E) schemes. Again the former scheme failed to separate the patients into prognosis-related

Table II. *Expression intensities of five probe sets linked to survival of 14 long-term and eight short-term survivors of acute myeloid leukemia.*

Affymetrix designation	Gene symbol	GenBank accession no.	Long-term survivors												
			ID026	ID035	ID087	ID093	ID139	ID142	ID174	ID195	ID226	ID227	ID239	ID266	ID269	ID270
217147_s_at	TRIM	AJ240085	22.2	22.4	5.3	42.9	26.5	4.9	0.9	3.6	14.2	6.4	43.0	11.0	30.5	27.9
203098_at	CDYL	AL050164	6.9	15.5	8.4	18.8	49.9	10.2	20.5	6.0	42.5	11.7	60.8	20.3	23.5	30.8
226333_at	IL6R	AV700030	16.3	34.0	68.4	39.2	20.2	52.3	60.5	80.3	54.2	60.6	49.4	107.4	50.6	24.4
243023_at		N34402	1.7	10.2	6.9	4.5	31.3	20.8	16.7	7.1	2.0	8.7	2.9	3.0	29.3	2.4
200663_at	CD63	NM_001780	170.0	73.0	132.4	181.5	74.4	97.7	60.4	94.2	112.9	112.8	102.1	68.2	82.0	76.6

Affymetrix designation	Gene symbol	GenBank accession no.	Short-term survivors								
			ID027	ID062	ID083	ID127	ID180	ID188	ID288	ID317	
217147_s_at	TRIM	AJ240085	1.3	7.3	1.1	2.9	2.7	5.0	1.5	4.1	
203098_at	CDYL	AL050164	48.5	60.1	35.1	30.7	44.3	67.4	33.2	47.0	
226333_at	IL6R	AV700030	177.2	146.2	127.5	72.5	120.7	85.7	61.8	70.1	
243023_at		N34402	28.8	33.5	33.4	23.4	24.5	10.8	19.7	19.5	
200663_at	CD63	NM_001780	57.9	65.9	67.7	52.7	61.8	49.4	62.5	76.6	

groups. In contrast, the GES scheme efficiently isolated the long-term survivors.

Discussion

In the present study, we attempted to develop a new classification scheme for AML based on the gene expression profiles of purified highly immature leukemic cells. Microarray analysis has proved effective for the prediction of prognosis in other hematological malignancies including diffuse large B cell lymphoma (DLBCL) (23-25) and acute lymphoblastic leukemia (ALL) (26, 27). The clinical specimens for these latter two disorders, however, appear to be more homogeneous than are those for AML. Lymphoma clones constitute most of the cell population within the affected lymph nodes of individuals with DLBCL and most ALL clones remain at an early precursor stage of the B or T cell lineage. The clinical specimens derived from individuals with DLBCL or ALL are thus probably representative of the corresponding malignant clones.

Caution is warranted, however, in the interpretation of microarray data for certain blood cell disorders. In Hodgkin's lymphoma, for example, the malignant cells constitute only a small proportion of cells within lymph nodes, most of which are inflammatory cells and normal lymphocytes. Hodgkin's lymphoma cells have thus been isolated with the use of laser-capture microdissection before microarray analysis (28, 29). Similar caution is required with AML, given the heterogeneity in both the proportion and differentiation ability of the blasts within BM. Indeed, our data indicated that so-called "leukemic blasts" are highly heterogeneous with regard to their differentiation ability, even within the BM of a single patient (Figure 1A), consistent with the notion of the presence of multiple types of LSC (12).

In the present study, statistical analysis of the gene expression profiles of $CD133^+$ HSC-like fractions resulted in the isolation of a very small number of outcome-predictor genes, including those for G protein-coupled receptor 56 (GPR56; GenBank accession number, NM_005682), ring finger protein 146 (RNF146; NM_030963), mitochondrial ribosomal protein S14 (MRPS14; NM_022100) and T cell receptor-interacting protein (TCRIM; NM_016388). Their predicted amino acid sequences indicate that GPR56 belongs to the family of cell surface proteins with seven transmembrane domains and that RNF146 participates in protein ubiquitination. MRPS14 is a component of the 28S subunit of mitochondrial ribosomes and contributes to protein synthesis in this organelle (30). TCRIM is a transmembrane protein that undergoes phosphorylation by Src family kinases (31). TCRIM potentially functions as a scaffold protein that recruits a variety of signaling proteins *via* its Src homology 2 (SH2) domain.

Table III. *The outcome predictor genes for acute myeloid leukemia (AML).*

Affymetrix designation	Gene symbol	GenBank accession no.	Parameter estimate	*P* value
203801_at	MRPS14	NM_022100	–2.30663	0.003
212070_at	GPR56	NM_005682	0.69679	0.0045
217147_s_at	TCRIM	NM_016388	–0.79050	0.0041
244517_x_at	RNF146	NM_030963	–0.97626	0.0018

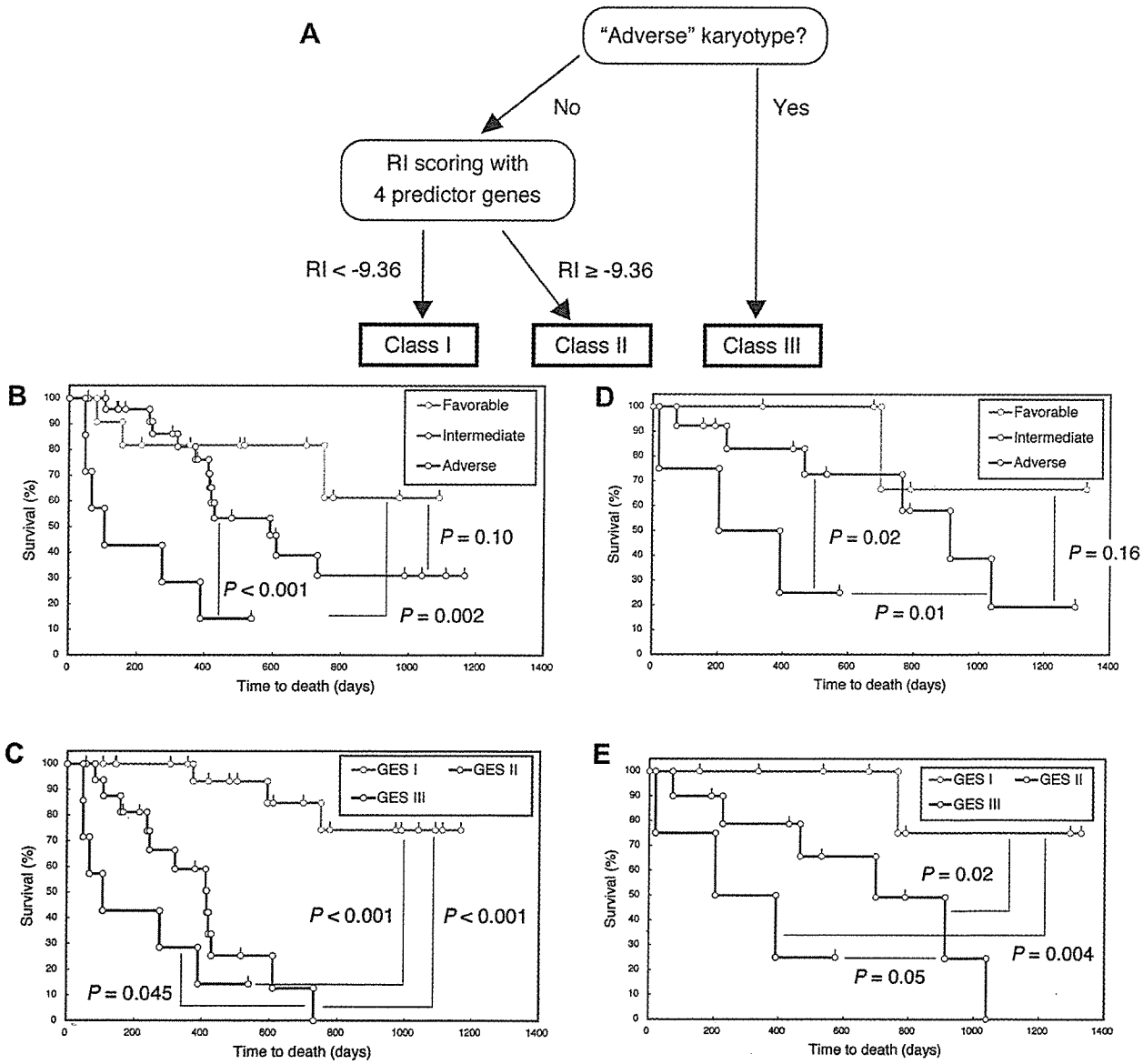

Figure 5. *The gene expression-based stratification (GES) system for acute myeloid leukemia (AML). A) Flow chart for GES classification of AML patients. B–E) Kaplan-Meier analysis of the 44 AML patients in the training set (B, C) and the 22 patients in the test set (D, E) classified according to karyotype-based stratification (B, D) or to the GES system (C, E).*

Table IV. *Expression intensities of 23 pobe sets linked to prognosis in the acute myeloid leukemia patients treated with standard chemotherapy.*

Affymetrix designation	Gene symbol	Genbank accession no.	Good prognosis																					
			ID026	ID035	ID076	ID087	ID093	ID107	ID139	ID142	ID174	ID183	ID195	ID226	ID227	ID239	ID265	ID266	ID269	ID270	ID277	ID278	ID279	ID314
37384_at	PPM1F	D13640	180.9	301.1	129.8	254.6	304.9	210.7	163.2	158.4	171.1	46	448.7	177.6	251.7	129.5	107.4	230.3	136.7	112.9	90	333.5	130	111.8
243579_at	MSI2	BF029215	84.5	40	21.9	170.4	39.7	32.3	30.3	11.4	59	21.3	97.1	47.5	62.5	42.8	35.3	72.5	18	12.5	15.9	208.2	20.2	47.2
228988_at	ZNF6	AU157017	10.6	16.2	7.7	28.8	55.5	57.2	2.4	4.9	138.3	5.5	8.7	20.3	22.1	18.2	4.9	25.2	4.5	1.9	5	57.7	4.6	5.8
228708_at		BF438386	23.2	10.5	54.5	44.7	16.6	20.1	39.6	10	38.8	57.9	12.9	22.5	59.2	97.7	89.4	49.8	60.7	63.3	112.4	171	32	3.2
225651_at	FLJ25157	BF431962	79.7	167	135	64.5	83.6	44.7	89.7	99.1	20.4	83.2	71.9	113	48.7	143	416.2	50.3	79.3	85.5	69.3	22.9	187.2	21.6
225351_at	HT011	AK027029	66.1	62.1	174.7	67.1	73.4	42.2	90.6	193.2	40.5	183.6	164.2	311.1	46.8	407.5	494.6	42.3	302	31	87.2	47	163.3	32.3
224516_s_at	HSPC195	BC006428	52.5	212.2	30.4	115.7	78.7	46.4	197.1	97.5	134	123	164.3	145	115.7	271.1	59.6	150.2	84.2	137.1	295.4	275	123.7	32.4
224367_at	DJ79P11.1	AF251053	68.5	44.3	9.2	18.1	29.4	158.7	5.8	9.9	188.8	26.4	15.8	27.7	12.4	10.8	37.9	97	4.6	7.2	14.4	177.4	5.4	14.2
219498_s_at	BCL11A	NM_1186	55.2	62.4	110.5	26.9	44	51	75.5	35.5	118.9	123.4	51.9	70.1	45.1	100.5	296.5	63.9	58.4	27.2	84.4	98.8	31.1	18.5
217975_at	LOC51186	NM_016303	58.4	32.6	6.1	3.3	27.9	40.9	5.5	16.1	54.4	20.9	22.5	18.9	31.2	6.7	244	55.5	7.3	6.6	9.7	208.2	6.5	86.9
215111_s_at	TSC22	AK027071	76.5	64	112.5	66.7	241.3	99.9	120.1	37.5	268.1	64.2	83.9	254.7	112.2	288	533.7	103.7	144.7	89.9	573.8	294.8	115.1	3.8
214651_s_at	HOXA9	U41813	14.7	14.6	7.5	55.6	185.4	163.1	7.8	11.9	134.3	3	4.4	19.2	61	8.1	190.7	114.6	0.6	2.3	118.6	401.7	0.9	19.9
212827_at	IGHM	X17115	753.6	151.3	35.5	222.3	136.6	142.3	47.2	57.6	214	36.7	62.8	23.8	138.8	24.8	69.9	49.1	21.6	20.8	205.3	185.4	55.4	48.7
211709_s_at	SCGF	BC005810	300	683.9	1184.4	268.5	552.3	3194.6	365.7	2041.3	245.1	2181.9	2493.3	2796.9	315.3	2800.3	373.8	432	788.9	517.7	643.6	2391.3	1150.7	4488.4
211341_at	POU4F1	L20433	59.6	612.2	233.8	28.9	16.6	5.5	29.9	813	11.4	607.5	1075	560.6	41	418.5	13.7	5.1	143	112.2	15.6	20.4	179.4	34.2
209905_at	HOXA9	AI246769	72.8	5.2	1.3	19	15.5	306.4	1.3	3.4	139.6	4.8	6	2.8	85.1	1.6	204.2	193.6	0.9	0.5	198.4	797.2	0.9	40
206478_at	KIAA0125	NM_014792	19	21.7	12.1	45.9	34	10.5	41.1	34.5	303.6	28.1	26.1	35.4	42.8	16.2	146.4	42	38.7	67.3	97.1	144.4	5.9	8.6
205609_at	ANGPT1	NM_001146	50	807.3	22.7	43.4	66.3	70.9	354.2	19.8	130.9	41.4	104.4	21.6	277.3	25.5	82.1	637.4	18	347.6	688.9	357	47	2.5
205608_s_at	ANGPT1	U83508	54.9	141.2	19.7	135.2	86.1	30.3	116.7	101.4	56.7	50.8	107.7	100	198.4	27.3	55.8	228.8	9	65.2	92.2	349.1	18	94.7
204949_at	ICAM3	NM_002162	36.9	49.7	84.3	65.1	52.5	27.9	163.9	24.3	369.8	58.3	70.8	135.4	82.2	98.6	51.4	158.3	159.5	181	186.2	341.7	169.1	34.7
204000_at	GNB5	NM_016194	11.9	37.8	13.6	19.8	63.7	9.9	87	19.3	27.1	31.6	41	39.6	21	2.7	25.1	7.4	62.9	55.1	29.4	69.4	9.3	82.6
203063_at	PPM1F	NM_014634	107.6	147.5	127.5	151.8	164.8	129.1	138.7	186.2	173.1	120	190.3	225.1	233.4	86.3	56.2	167.8	117.3	97.1	78.4	239	65.7	86.2
201315_x_at	IFITM2	NM_006435	217.8	156.4	339.9	286.1	437.7	201.2	55.2	64.7	268.1	67.3	139.9	218.8	132.7	279.4	41.7	121	84.5	93.9	49.3	148.2	320.1	134.4

continued

Table IV. *continued*

Affymetrix designation	Gene symbol	Genbank accession no.	Poor prognosis																					
			ID027	ID042	ID054	ID062	ID083	ID127	ID188	ID288	ID313	ID317	ID325	ID349	ID380	ID388	ID402	ID409	ID413	ID414	ID415	ID416	ID418	ID427
37384_at	PPM1F	D13640	222.4	415.7	235.3	199.8	165.9	204	275.8	274.9	339.4	394.5	518.6	281.9	268.6	317.5	160.1	444	240.2	134.5	193	180	276.7	191.9
243579_at	MSI2	BF029215	38.5	118.9	62.3	90.9	19.5	49.2	156.3	293.6	80.7	17.3	41.5	159.3	222.8	70.7	44.5	168.9	34.9	123.8	125.1	170.6	456.3	100
228988_at	ZNF6	AU157017	148.9	141.8	199	11.7	17.6	116.9	15.8	218.3	55.8	12.5	26.6	300.3	68	25.9	3.2	267.4	5.5	139	286.9	60	18.8	41.4
228708_at		BF438386	127.2	196.3	430.7	37.8	58.7	137.7	137	118.6	66.2	57.7	44.8	82.6	28	99.3	18.5	358.5	12.5	117.1	18.4	149.4	33.4	129.7
225651_at	FLJ25157	BF431962	62.9	47.7	11.8	86	18.7	60.5	26.1	19.1	56.5	93.7	23.8	39	97.8	92.2	30.4	56.7	45.7	33.7	54.7	25.9	88.7	74.8
225351_at	HT011	AK027029	64.6	55.2	26.1	122.5	48	61.5	106.2	21	93.5	91.7	46.7	22.8	68.6	96.5	58	74.6	27	43.8	63.6	20.7	28	72.6
224516_s_at	HSPC195	BC006428	295.5	158.1	466.3	174.2	208.9	241.3	62.4	199.8	168.4	131.8	107	127.4	223	387.3	138.4	166.9	110.7	165.6	172.2	175.6	207.8	146.2
224367_at	DJ79P11.1	AF251053	188.6	343.3	173.7	8.1	93.5	345	56.7	202.8	45.3	5	24	475.1	307.3	38.6	3.5	363.7	12	259.9	273.9	136.9	109.7	68.8
219498_s_at	BCL11A	NM_018014	106.4	233.2	108.4	237.3	135.8	66.6	90.8	80.4	182.9	83.7	54.5	169	101.5	238.5	71.7	229.2	66.3	155.1	114.6	87.3	201.6	54.2
217975_at	LOC51186	NM_016303	208	191.6	111.8	10.1	64.9	157.5	6.5	88.4	303.8	5.9	36.8	350	173.9	124.6	7.7	75.5	38.8	163.6	291	102.1	227.1	160.1
215111_s_at	TSC22	AK027071	366.5	709.6	696.9	562.8	281.6	255.7	143.3	198.4	282.8	115.8	114.9	904	195.1	669.3	50.8	316.5	68.2	233.1	289	143.8	258.5	215.9
214651_s_at	HOXA9	U41813	293.6	379.5	166.6	125.8	121.9	121.7	34.3	326.8	180.5	14.7	247.4	231.1	158.6	157.3	1.6	389	4.9	159.5	215.6	108.1	65.5	324
212827_at	IGHM	X17115	179.6	337.3	272	278.3	204.9	128.4	40.8	303.7	200.1	25.7	609.8	371.1	1002.5	471.9	19.6	120.2	62.4	393	224.2	456.1	124.2	295.4
211709_s_at	SCGF	BC005810	91.2	459.8	47.1	857.1	494	313.7	1762.7	298.9	1004.1	899.4	19.2	225.2	796.7	2637.8	66.2	361.6	866.5	90.2	69	453.1	183.7	679.3
211341_at	POU4F1	L20433	2	1.8	0.8	12.3	4	7.2	1089.2	9.8	22.5	790.7	12	16.3	7.5	49.2	39.3	95.6	2.5	13.1	13.4	17.5	21.3	55.8
209905_at	HOXA9	AI246769	428	382.5	253.7	99.4	152.4	148.7	9.2	125.7	282.8	9.6	77.4	502.6	129.7	96.6	1.4	356.1	0.7	262.6	415.7	202.3	121.2	477.9
206478_at	KIAA0125	NM_014792	517.3	198.9	584.7	127.7	317.1	39.8	27.4	31.2	94.3	43.3	39.7	185.6	90.9	84.5	33.7	144.8	16.7	99.1	79.5	49.5	40.1	105.4
205609_at	ANGPT1	NM_001146	1554.3	1007.2	524.9	27.5	264.3	847.5	16.3	308.5	651.8	93.5	8.7	223.6	882.5	1067.1	306.5	362.8	123.5	261	606.1	236.6	988.8	317.3
205608_s_at	ANGPT1	U83508	158.9	253.2	218.4	84.6	131.4	28.4	38	447.3	157.9	95.5	116.6	143.1	616	304.3	107.5	328.3	52.9	141	265.2	247.5	269	415.4
204949_at	ICAM3	NM_002162	104.8	209.3	156.5	119.2	271.2	316.1	38.4	217.9	358.6	109.4	136.5	382.6	487.1	305.4	265.4	291.4	233.4	245	245.5	118.9	44.7	295.6
204000_at	GNB5	NM_016194	15.4	91.7	57.4	26.4	58.7	140.5	36.3	40.6	83.2	90.9	61.7	48.3	35.6	129.1	30	20	151.1	33.3	76.8	75.7	654.9	119.8
203063_at	PPM1F	NM_014634	187.6	318.6	216.8	132.2	166.5	126.5	189.9	278.2	263.3	128.3	439.2	240.2	163	280.5	131.1	265.3	175.6	129.1	144.6	152.2	142.9	246.5
201315_x_at	IFITM2	NM_006435	274.8	291.4	464.2	492.5	374.1	390.3	127.1	115.3	299.1	245.8	670	379.9	176.6	337	219.7	177	235.3	158.9	187.5	68.6	185.7	170.9

ANOVA ($p<0.01$) and effect size selection (≥50 U) identified 31 probe sets, expression of which differed between individuals who failed to enter initial complete remission after the standard chemotherapy (poor prognosis) and those who remained at complete remission for >1 year after the standard chemotherapy (good prognosis). The Cox proportional hazard model was applied to such probe sets to isolate 23 probe sets whose expression levels correlated ($p<0.05$) with survival time. The expression intensities of these 23 probe sets are shown.

Recent microarray analyses of BM MNCs from AML patients identified a cluster of ~100 genes whose expression patterns discriminated among AML subtypes (19) and 133 genes whose expression patterns were predictive of clinical outcome (32). Both *GPR56* and *TCRIM* were among the former group of genes.

Given that our data set was obtained with purified HSC-like fractions, it should prove informative with regard to characterization, through various approaches, of undifferentiated leukemic clones (probably including LSCs). For example, comparison between the individuals with good and poor prognosis among the 66 AML patients who underwent standard chemotherapy revealed preferential expression of *ANGPT1* in the latter group (Table IV); this gene encodes an angiogenic factor (angiopoietin 1) and is frequently overexpressed in a wide variety of human cancers (33, 34). An increased level of expression of *TEK*, which encodes a receptor for ANGPT1, was also detected in the blasts of ~10% of all 99 study subjects, some of whom overexpressed both *TEK* and *ANGPT1* (data not shown). These data suggest that an autocrine loop consisting of ANGPT1 and TEK might contribute to the malignant transformation in AML.

In contrast to the requirement for quantitation of the expression of >100 genes in the previously described approaches to prognosis prediction with BM MNCs from AML patients (19, 32), our GES system relies on determination of the expression levels of only four genes. Analysis of such a small number of genes is within the scope of an assay based on simple methodology, such as multiplex PCR. Although the GES system requires purification of $CD133^+$ cells, a combination of karyotyping and multiplex PCR is relatively straightforward even in current clinical settings. A large prospective study is now needed to verify whether individuals with AML of GES class I should be treated by standard chemotherapies, and those with AML of GES class II or III should receive more aggressive treatments such as BM transplantation.

Acknowledgements

We thank P. Simon for helpful discussion and suggestions. This work was supported, in part, by grants for Research on Human Genome and Tissue Engineering and for Third-Term Comprehensive Control Research for Cancer from the Ministry of Health, Labor, and Welfare of Japan, as well as by a grant for Scientific Research on Priority Areas "Applied Genomics" from the Ministry of Education, Culture, Sports, Science and Technology of Japan.

References

1 Byrd JC, Mrozek K, Dodge RK, Carroll AJ, Edwards CG, Arthur DC, Pettenati MJ, Patil SR, Rao KW, Watson MS, Koduru PR, Moore JO, Stone RM, Mayer RJ, Feldman EJ, Davey FR, Schiffer CA, Larson RA and Bloomfield CD: Pretreatment cytogenetic abnormalities are predictive of induction success, cumulative incidence of relapse, and overall survival in adult patients with *de novo* acute myeloid leukemia: results from Cancer and Leukemia Group B (CALGB 8461). Blood *100*: 4325-4336, 2002.

2 Bennett JM, Catovsky D, Daniel MT, Flandrin G, Galton DA, Gralnick HR and Sultan C: Proposed revised criteria for the classification of acute myeloid leukemia. A report of the French-American-British Cooperative Group. Ann Intern Med *103*: 620-625, 1985.

3 Goasguen JE, Matsuo T, Cox C and Bennett JM: Evaluation of the dysmyelopoiesis in 336 patients with *de novo* acute myeloid leukemia: major importance of dysgranulopoiesis for remission and survival. Leukemia *6*: 520-525, 1992.

4 Grimwade D, Walker H, Oliver F, Wheatley K, Harrison C, Harrison G, Rees J, Hann I, Stevens R, Burnett A and Goldstone A: The importance of diagnostic cytogenetics on outcome in AML: analysis of 1,612 patients entered into the MRC AML 10 trial. The Medical Research Council Adult and Children's Leukaemia Working Parties. Blood *92*: 2322-2333, 1998.

5 Jaffe ES, Harris NL, Stein H and Vardiman JW: Pathology and Genetics of Tumours of Haematopoietic and Lymphoid Tissues. Lyon, IARC Press, 2001.

6 Liu ET and Karuturi KR: Microarrays and clinical investigations. N Engl J Med *350*: 1595-1597, 2004.

7 Miyazato A, Ueno S, Ohmine K, Ueda M, Yoshida K, Yamashita Y, Kaneko T, Mori M, Kirito K, Toshima M, Nakamura Y, Saito K, Kano Y, Furusawa S, Ozawa K and Mano H: Identification of myelodysplastic syndrome-specific genes by DNA microarray analysis with purified hematopoietic stem cell fraction. Blood *98*: 422-427, 2001.

8 Ohmine K, Ota J, Ueda M, Ueno S-i, Yoshida K, Yamashita Y, Kirito K, Imagawa S, Nakamura Y, Saito K, Akutsu M, Mitani K, Kano Y, Komatsu N, Ozawa K and Mano H: Characterization of stage progression in chronic myeloid leukemia by DNA microarray with purified hematopoietic stem cells. Oncogene *20*: 8249-8257, 2001.

9 Hin AH, Miraglia S, Zanjani ED, Almeida-Porada G, Ogawa M, Leary AG, Olweus J, Kearney J and Buck DW: AC133, a novel marker for human hematopoietic stem and progenitor cells. Blood *90*: 5002-5012, 1997.

10 Peichev M, Naiyer AJ, Pereira D, Zhu Z, Lane WJ, Williams M, Oz MC, Hicklin DJ, Witte L, Moore MA and Rafii S: Expression of VEGFR-2 and AC133 by circulating human CD34(+) cells identifies a population of functional endothelial precursors. Blood *95*: 952-958, 2000.

11 Bonnet D and Dick JE: Human acute myeloid leukemia is organized as a hierarchy that originates from a primitive hematopoietic cell. Nat Med *3*: 730-737, 1997.

12 Hope KJ, Jin L and Dick JE: Acute myeloid leukemia originates from a hierarchy of leukemic stem cell classes that differ in self-renewal capacity. Nat Immunol *5*: 738-743, 2004.

13 Singh SK, Hawkins C, Clarke ID, Squire JA, Bayani J, Hide T, Henkelman RM, Cusimano MD and Dirks PB: Identification of human brain tumour initiating cells. Nature *432*: 396-401, 2004.

14 Van Gelder RN, von Zastrow ME, Yool A, Dement WC, Barchas JD and Eberwine JH: Amplified RNA synthesized from limited quantities of heterogeneous cDNA. Proc Natl Acad Sci USA *87*: 1663-1667, 1990.

15 Oshima Y, Ueda M, Yamashita Y, Choi YL, Ota J, Ueno S, Ohki R, Koinuma K, Wada T, Ozawa K, Fujimura A and Mano H: DNA microarray analysis of hematopoietic stem cell-like fractions from individuals with the M2 subtype of acute myeloid leukemia. Leukemia *17*: 1990-1997, 2003.
16 Fellenberg K, Hauser NC, Brors B, Neutzner A, Hoheisel JD and Vingron M: Correspondence analysis applied to microarray data. Proc Natl Acad Sci USA *98*: 10781-10786, 2001.
17 Alon U, Barkai N, Notterman DA, Gish K, Ybarra S, Mack D and Levine AJ: Broad patterns of gene expression revealed by clustering analysis of tumor and normal colon tissues probed by oligonucleotide arrays. Proc Natl Acad Sci USA *96*: 6745-6750, 1999.
18 Ichikawa N, Kitano K, Ito T, Nakazawa T, Shimodaira S, Ishida F and Kiyosawa K: Abnormal proliferation of CD4-CD8+ gammadelta+ T cells with chromosome 6 anomaly: role of Fas ligand expression in spontaneous regression of the cells. Am J Hematol *60*: 305-308, 1999.
19 Valk PJ, Verhaak RG, Beijen MA, Erpelinck CA, Barjesteh van Waalwijk van Doorn-Khosrovani S, Boer JM, Beverloo HB, Moorhouse MJ, van der Spek PJ, Lowenberg B and Delwel R: Prognostically useful gene-expression profiles in acute myeloid leukemia. N Engl J Med *350*: 1617-1628, 2004.
20 Wheatley K, Burnett AK, Goldstone AH, Gray RG, Hann IM, Harrison CJ, Rees JK, Stevens RF and Walker H: A simple, robust, validated and highly predictive index for the determination of risk-directed therapy in acute myeloid leukaemia derived from the MRC AML 10 trial. United Kingdom Medical Research Council's Adult and Childhood Leukaemia Working Parties. Br J Haematol *107*: 69-79, 1999.
21 Cox DR: Regression models and life tables. J R Stat Soc *34*: 187-220, 1972.
22 Beer DG, Kardia SL, Huang CC, Giordano TJ, Levin AM, Misek DE, Lin L, Chen G, Gharib TG, Thomas DG, Lizyness ML, Kuick R, Hayasaka S, Taylor JM, Iannettoni MD, Orringer MB and Hanash S: Gene-expression profiles predict survival of patients with lung adenocarcinoma. Nat Med *8*: 816-824, 2002.
23 Alizadeh AA, Eisen MB, Davis RE, Ma C, Lossos IS, Rosenwald A, Boldrick JC, Sabet H, Tran T, Yu X, Powell JI, Yang L, Marti GE, Moore T, Hudson J Jr, Lu L, Lewis DB, Tibshirani R, Sherlock G, Chan WC, Greiner TC, Weisenburger DD, Armitage JO, Warnke R, Levy R, Wilson W, Grever MR, Byrd JC, Botstein D, Brown PO and Staudt LM: Distinct types of diffuse large B-cell lymphoma identified by gene expression profiling. Nature *403*: 503-511, 2000.
24 Rosenwald A, Wright G, Chan WC, Connors JM, Campo E, Fisher RI, Gascoyne RD, Muller-Hermelink HK, Smeland EB, Giltnane JM, Hurt EM, Zhao H, Averett L, Yang L, Wilson WH, Jaffe ES, Simon R, Klausner RD, Powell J, Duffey PL, Longo DL, Greiner TC, Weisenburger DD, Sanger WG, Dave BJ, Lynch JC, Vose J, Armitage JO, Montserrat E, Lopez-Guillermo A, Grogan TM, Miller TP, LeBlanc M, Ott G, Kvaloy S, Delabie J, Holte H, Krajci P, Stokke T and Staudt LM: The use of molecular profiling to predict survival after chemotherapy for diffuse large-B-cell lymphoma. N Engl J Med *346*: 1937-1947, 2002.
25 Shipp MA, Ross KN, Tamayo P, Weng AP, Kutok JL, Aguiar RC, Gaasenbeek M, Angelo M, Reich M, Pinkus GS, Ray TS, Koval MA, Last KW, Norton A, Lister TA, Mesirov J, Neuberg DS, Lander ES, Aster JC and Golub TR: Diffuse large B-cell lymphoma outcome prediction by gene-expression profiling and supervised machine learning. Nat Med *8*: 68-74, 2002.
26 Ferrando AA, Neuberg DS, Staunton J, Loh ML, Huard C, Raimondi SC, Behm FG, Pui CH, Downing JR, Gilliland DG, Lander ES, Golub TR and Look AT: Gene expression signatures define novel oncogenic pathways in T cell acute lymphoblastic leukemia. Cancer Cell *1*: 75-87, 2002.
27 Yeoh EJ, Ross ME, Shurtleff SA, Williams WK, Patel D, Mahfouz R, Behm FG, Raimondi SC, Relling MV, Patel A, Cheng C, Campana D, Wilkins D, Zhou X, Li J, Liu H, Pui CH, Evans WE, Naeve C, Wong L and Downing JR: Classification, subtype discovery, and prediction of outcome in pediatric acute lymphoblastic leukemia by gene expression profiling. Cancer Cell *1*: 133-143, 2002.
28 Kapp U, Yeh WC, Patterson B, Elia AJ, Kagi D, Ho A, Hessel A, Tipsword M, Williams A, Mirtsos C, Itie A, Moyle M and Mak TW: Interleukin 13 is secreted by and stimulates the growth of Hodgkin and Reed-Sternberg cells. J Exp Med *189*: 1939-1946, 1999.
29 Skinnider BF, Elia AJ, Gascoyne RD, Trumper LH, von Bonin F, Kapp U, Patterson B, Snow BE and Mak TW: Interleukin 13 and interleukin 13 receptor are frequently expressed by Hodgkin and Reed-Sternberg cells of Hodgkin lymphoma. Blood *97*: 250-255, 2001.
30 Cavdar Koc E, Burkhart W, Blackburn K, Moseley A and Spremulli LL: The small subunit of the mammalian mitochondrial ribosome. Identification of the full complement of ribosomal proteins present. J Biol Chem *276*: 19363-19374, 2001.
31 Bruyns E, Marie-Cardine A, Kirchgessner H, Sagolla K, Shevchenko A, Mann M, Autschbach F, Bensussan A, Meuer S and Schraven B: T cell receptor (TCR) interacting molecule (TRIM), a novel disulfide-linked dimer associated with the TCR-CD3-zeta complex, recruits intracellular signaling proteins to the plasma membrane. J Exp Med *188*: 561-575, 1998.
32 Bullinger L, Dohner K, Bair E, Frohling S, Schlenk RF, Tibshirani R, Dohner H and Pollack JR: Use of gene-expression profiling to identify prognostic subclasses in adult acute myeloid leukemia. N Engl J Med *350*: 1605-1616, 2004.
33 Shim WS, Teh M, Bapna A, Kim I, Koh GY, Mack PO and Ge R: Angiopoietin 1 promotes tumor angiogenesis and tumor vessel plasticity of human cervical cancer in mice. Exp Cell Res *279*: 299-309, 2002.
34 Giuliani N, Colla S, Lazzaretti M, Sala R, Roti G, Mancini C, Bonomini S, Lunghi P, Hojden M, Genestreti G, Svaldi M, Coser P, Fattori PP, Sammarelli G, Gazzola GC, Bataille R, Almici C, Caramatti C, Mangoni L and Rizzoli V: Proangiogenic properties of human myeloma cells: production of angiopoietin-1 and its potential relationship to myeloma-induced angiogenesis. Blood *102*: 638-645, 2003.

Received April 1, 2006
Accepted May 15, 2006

Signals from intra-abdominal fat modulate insulin and leptin sensitivity through different mechanisms: Neuronal involvement in food-intake regulation

Tetsuya Yamada,[1,7] Hideki Katagiri,[2,7,*] Yasushi Ishigaki,[1,7] Takehide Ogihara,[2] Junta Imai,[1,2] Kenji Uno,[1,2] Yutaka Hasegawa,[1,2] Junhong Gao,[1,2] Hisamitsu Ishihara,[1] Akira Niijima,[3] Hiroyuki Mano,[4] Hiroyuki Aburatani,[5] Tomoichiro Asano,[6] and Yoshitomo Oka[1]

[1] Division of Molecular Metabolism and Diabetes
[2] Division of Advanced Therapeutics for Metabolic Diseases, Center for Translational and Advanced Animal Research
Tohoku University Graduate School of Medicine, Sendai 980-8575, Japan
[3] Niigata University School of Medicine, Niigata 951-8150, Japan
[4] Division of Functional Genomics, Jichi Medical School, Kawachi-gun, Tochigi 329-0498, Japan
[5] Research Center for Advanced Science and Technology, University of Tokyo, Tokyo 153-8904, Japan
[6] Department of Physiological Chemistry and Metabolism, University of Tokyo, Tokyo 113-8655, Japan
[7] These authors contributed equally to this work.
*Correspondence: katagiri-tky@umin.ac.jp

Summary

Intra-abdominal fat accumulation is involved in development of the metabolic syndrome, which is associated with insulin and leptin resistance. We show here that ectopic expression of very low levels of uncoupling protein 1 (UCP1) in epididymal fat (Epi) reverses both insulin and leptin resistance. UCP1 expression in Epi improved glucose tolerance and decreased food intake in both diet-induced and genetically obese mouse models. In contrast, UCP1 expression in Epi of leptin-receptor mutant mice did not alter food intake, though it significantly decreased blood glucose and insulin levels. Thus, hypophagia induction requires a leptin signal, while the improved insulin sensitivity appears to be leptin independent. In wild-type mice, local-nerve dissection in the epididymis or pharmacological afferent blockade blunted the decrease in food intake, suggesting that afferent-nerve signals from intra-abdominal fat tissue regulate food intake by modulating hypothalamic leptin sensitivity. These novel signals are potential therapeutic targets for the metabolic syndrome.

Introduction

The explosive increase in obesity has become a major public health concern in most industrialized countries (Flier, 2004; Friedman, 2003). Insulin resistance is a fundamental contributor to the metabolic syndrome associated with type 2 diabetes, hypertension, hyperlipidemia, and atherosclerosis. Major advancements in this field include the discoveries of adipocyte-derived humoral factors, such as leptin (Friedman and Halaas, 1998). Leptin conveys energy-storage information from adipose tissue to the central nervous system, leading to food-intake suppression. However, in patients with ordinary obesity, serum leptin levels are increased in proportion to body fat (Considine et al., 1996), but the responses to leptin are impaired (Heymsfield et al., 1999), which defines a state of leptin resistance. Leptin resistance also contributes to the development of obesity and obesity-related metabolic disorders.

Fat accumulation in intra-abdominal fat tissue is involved in development of the metabolic syndrome (Bjorntorp, 1992; Matsuzawa et al., 1995) associated with insulin and leptin resistance (Friedman, 2003). Therefore, in this study, to examine whether the metabolic changes in intra-abdominal fat tissue affect insulin and leptin resistance as well as systemic glucose metabolism, we attempted to express uncoupling protein 1 (UCP1), which functions to dissipate energy as heat (Klingenberg and Huang, 1999), in epididymal fat tissue (Epi) in mice with obesity and diabetes.

Results and discussion

C57BL/6 mice were subjected to direct injection of the UCP1 adenovirus vector into Epi (UCP1 mice) after the development of diabetes associated with obesity in response to high-fat chow preloading for 4 weeks. Mice given the LacZ adenovirus were used as controls (LacZ mice). Immunoblotting detected adenovirus-mediated UCP1 expression in Epi (see Figure S1A in the Supplemental Data available with this article online), and this expression was restricted to Epi (Fig. S1A). UCP1 expression in Epi was detectable on the first day after adenoviral injection and was increased on day 3 but had fallen to very low levels by day 7 (Figure S1B). However, expression levels were far below those of endogenous protein in BAT: on day 3, approximately 5% per unit weight protein (Figure S1B). UCP1 expression was restricted to very limited portions of the tissue (left panel of Figure 1B). Judging from the intensity of immunostaining, UCP1 expression levels in UCP1-expressing white adipocytes did not reach those in brown adipocytes (right panel of Figure 1B). UCP1-expressing adipocytes were significantly smaller than UCP1-nonexpressing adipocytes in the same tissue (Figure 1C), suggesting enhanced metabolism in the former.

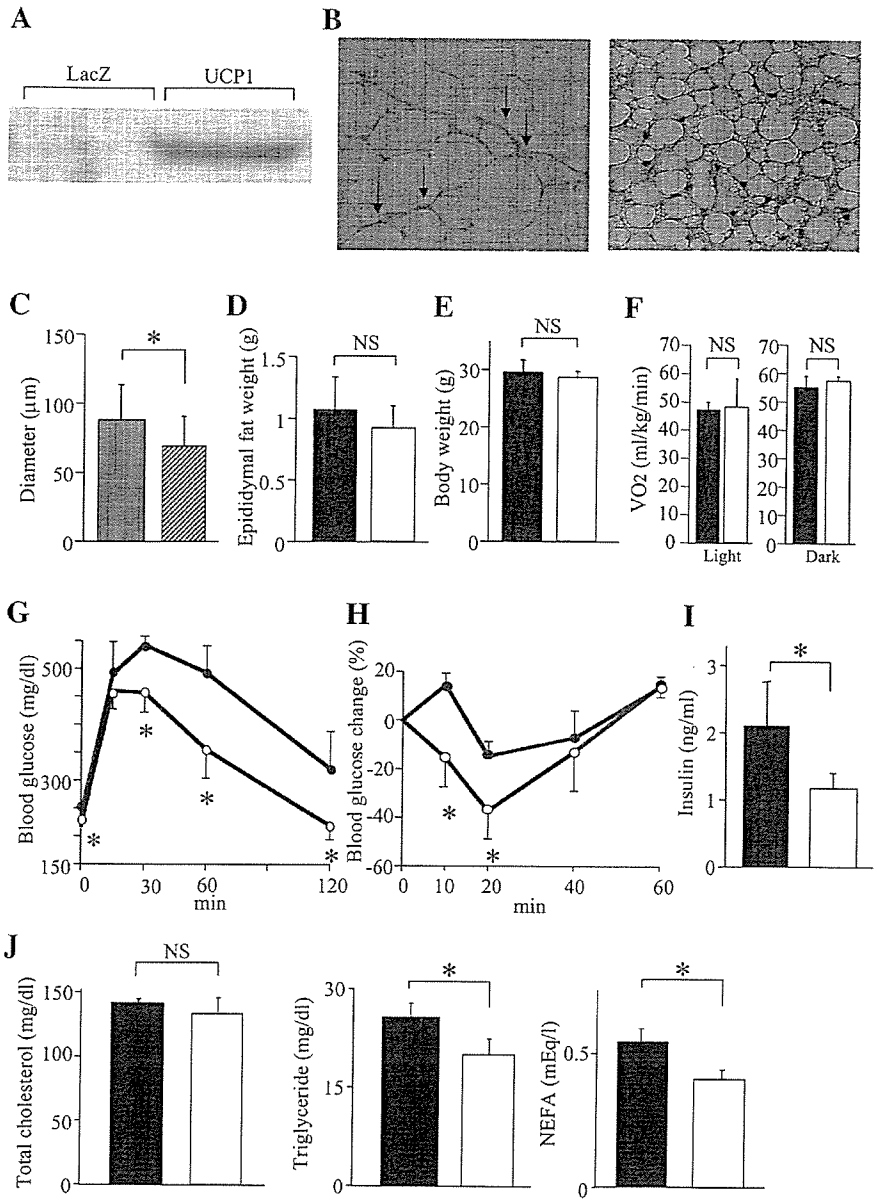

Figure 1. UCP1 expression in Epi improved glucose tolerance and insulin sensitivity

A) Immunoblotting, with anti-UCP1 antibody, of Epi extracts from LacZ and UCP1 mice on day 3 after adenoviral administration.

B) Immunohistochemistry, with anti-UCP1 antibody, of Epi (left panel) and BAT (right panel) sections from a UCP1 mouse on day 3 after adenoviral administration. These two samples were immunostained under the same conditions.

C) Diameters of UCP1-nonexpressing (gray bar) and UCP1-expressing (hatched bar) adipocytes in Epi from UCP1 mice on day 3 after adenoviral administration.

D–J) Epididymal fat weights (**D**), body weights (**E**), resting oxygen consumption during light and dark phase (**F**), and metabolic parameters (**G–J**) of LacZ mice (black bars) and UCP1 mice (white bars) on day 3 after adenoviral administration. Glucose-tolerance (**G**) and insulin-tolerance tests (**H**) were performed on day 3. Data in (**H**) are expressed as percentages of the blood glucose levels immediately before intraperitoneal insulin loading. Serum insulin levels (**I**) and serum lipid parameters ([**J**]; left: total cholesterol, middle: triglyceride, right: free fatty acids) were measured after a 10 hr fast (n = 6 per group). Data are presented as means ± SD (n = 6 per group). *$p < 0.05$ by unpaired t test.

We further confirmed enhanced metabolism by adenoviral UCP1 expression using 3T3-L1 adipocytes. UCP1 expression decreased intracellular ATP concentrations (Figure S1C) and increased levels of peroxisome proliferator-activated receptor γ coactivator (PGC) 1α and cytochrome c expression (Figure S1D). Thus, exogenous UCP1 was functionally active, resulting in increased mitochondrial biosynthesis in adipocytes.

However, neither total Epi weights nor body weights differed between LacZ and UCP1 mice on day 3 after adenoviral administration (Figures 1D and 1E). Oxygen consumption was not affected by UCP1 expression in Epi during either the light or the dark phase (Figure 1F), also reflecting the very limited UCP1 expression. Therefore, to avoid the secondary effects of bodyweight change, we analyzed metabolic parameters on day 3. To our surprise, however, even very limited UCP1 expression in Epi resulted in marked changes in metabolic phenotype.

Glucose- and insulin-tolerance tests indicated marked improvements in glucose tolerance and insulin sensitivity (Figures 1G and 1H). Fasting blood glucose (Figure 1G) and insulin (Figure 1I) levels were significantly lower in UCP1 mice, further confirming improved insulin sensitivity. In addition, serum lipid parameters, including triglycerides and free fatty acids (Figure 1J), were also improved with UCP1 expression in Epi. Thus, limited regional expression of UCP1 in Epi markedly improved systemic insulin resistance, resulting in improvement of diabetes and dyslipidemia.

Next, we measured serum adipocytokine levels (Figure 2A). Adiponectin and tumor necrosis factor α levels were not significantly altered. In contrast, serum leptin was markedly decreased, by 46%, with UCP1 expression in Epi. Although intra-abdominal fat-tissue weights were unaltered or only very slightly decreased in UCP1 mice (Figure 1D and Figure S1E),

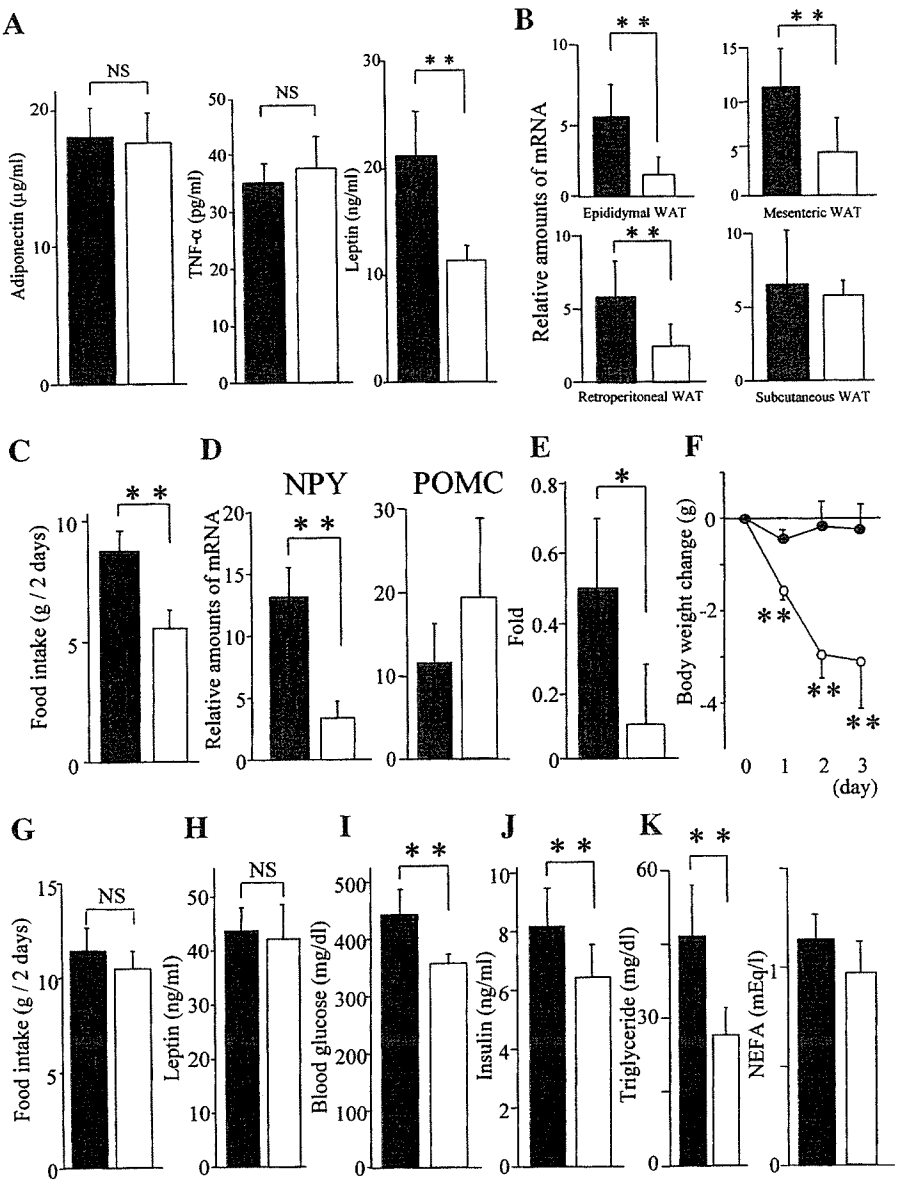

Figure 2. UCP1 expression in Epi improved leptin sensitivity

A–F) LacZ (black bars) or UCP1 (white bars) adenovirus was injected into Epi of mice with dietary obesity.

A) Serum adipocytokine levels (left: adiponectin, middle: TNFα, right: leptin) in LacZ mice and UCP1 mice after a 10 hr fast on day 3 after adenoviral administration.

B) Relative amounts of leptin mRNA in adipose tissues.

C) Total food intakes on days 2 and 3 after adenoviral administration.

D) Relative amounts of neuropeptide Y (left) and proopiomelanocortin (right) mRNA were measured by quantitative RT-PCR using total RNA obtained from the hypothalamus on day 2 after adenoviral administration. Data were corrected with β-actin as the standard (**B** and **D**).

E and F) Leptin-tolerance tests were performed on day 3 after adenoviral administration. Data were expressed as ratios to the food intakes of vehicle-treated mice (**E**). Mice were weighed at 12 hr after each daily injection of leptin or vehicle (**F**).

G–K) LacZ (black bars) or UCP1 (white bars) adenovirus was injected into Epi of db/db mice.

G) Total food intakes on days 2 and 3 after adenoviral administration are presented.

H–K) Blood leptin (**H**), glucose (**I**), and insulin (**J**) levels and serum lipid parameters ([**K**]; left: triglyceride, right: free fatty acids) of db/db mice were measured after a 10 hr fast. Data are presented as means ± SD (n = 8 per group). *p < 0.05; **p < 0.01 by unpaired t test.

leptin mRNA expression was markedly decreased in intra-abdominal fat tissues (Figure 2B). Thus, the effects of UCP1 expression in Epi are also exerted in fat tissues other than those injected with the adenovirus. Food intake was significantly suppressed (Figure 2C), indicating that hypothalamic leptin sensitivity was markedly improved despite the lack of significant changes in body weights. Decreased leptin expression in several adipose tissues suggests efferent sympathetic nerve activation, which also supports leptin signal enhancement.

Administration of green fluorescent protein-adenovirus exerted minimal metabolic effects (Figures S1F–S1J). On day 7, when adenoviral UCP1 expression was markedly decreased (Figure S1B), blood glucose, insulin, and leptin levels did not differ between the UCP1 and LacZ mice (Figure S2). In addition, we confirmed the metabolic effects of UCP1 expression in Epi using three other obese models: AKR mice on high-fat chow and KK mice and KK-Ay mice on normal chow. In these three models, similar metabolic impacts were observed with UCP1 adenovirus administration into Epi (Figure S3). Thus, UCP1 expression in Epi exerts acute, beneficial metabolic effects in both diet-induced and genetically obese models.

Increased leptin signals in the hypothalamus induced by UCP1 expression in Epi were further confirmed by changed levels of hypothalamic neuropeptide expression in UCP1 mice on day 3 after adenoviral administration. Real-time RT-PCR revealed adipose UCP1 expression to significantly decrease expression of neuropeptide Y, an orexigenic neuropeptide, while tending to increase that of proopiomelanocortin, a precursor of an anorexigenic neuropeptide, in the hypothalamus (Figure 2D).

To directly test whether leptin sensitivity was improved, we performed leptin-tolerance tests. When leptin was injected intraperitoneally into fasting mice on day 3, leptin-induced food-intake inhibition was far more profound in UCP1 mice than in LacZ mice (Figure 2E). In addition, when leptin was given daily, body weights were significantly decreased (Figure 2F). Thus,

even very limited UCP1 expression in Epi exerts a remote therapeutic effect on hypothalamic leptin resistance, which had already developed in response to preloading with high-fat chow. Transgenic overexpression of UCP1 (Kopecky et al., 1995) and rather minor induction of UCP1 in white adipose tissue (Cederberg et al., 2001; Leonardsson et al., 2004; Tsukiyama-Kohara et al., 2001; Um et al., 2004) result in resistance to high-fat-diet-induced obesity but do not reportedly cause hypophagia. In this study, however, we expressed UCP1 after the development of obesity and leptin resistance and were thus able to observe acute, beneficial effects, i.e., improved leptin sensitivity, which would be difficult to detect using congenitally UCP1-overexpressing mice.

Increased leptin sensitivity is likely to be involved in the phenotype of UCP1 mice. If this is the case, at least some of the phenotypic features of UCP1 mice would presumably be absent in mice lacking the hypothalamic leptin signal. To test this, UCP1 or LacZ adenovirus was injected into Epi of db/db mice, leptin-receptor Ob-Rb mutants. Food intake (Figure 2G) and serum leptin (Figure 2H) did not differ between LacZ-expressing and UCP1-expressing db/db mice. These findings confirm that the effect of UCP1 expression in Epi on food intake is leptin-signal dependent. On the other hand, UCP1 expression in Epi of db/db mice caused small but significant decreases in blood glucose (Figure 2I), insulin (Figure 2J), and triglyceride (Figure 2K) levels, as well as tending to decrease serum free-fatty-acid levels (Figure 2K). These findings demonstrate that UCP1 expression in Epi improves insulin sensitivity, in part, independently of leptin signaling.

To eliminate the secondary effects of reduced food intake, pair-feeding experiments were performed using C57BL/6 wild-type mice (Figure S4). Pair feeding did not significantly alter the body weights of LacZ mice. Fasting blood glucose did not differ between UCP1 mice and pair-fed LacZ mice, but after glucose loading, blood glucose levels were significantly lower in UCP1 mice. In addition, serum insulin and leptin levels were significantly lower in UCP1 mice than in pair-fed LacZ mice. Taken together with the results obtained using db/db mice, the improved insulin sensitivity induced by UCP1 expression in Epi appears not to be mediated solely by decreased food intake.

The same amounts of recombinant adenovirus encoding UCP1 were directly injected into subcutaneous fat tissues in the flank of C57BL/6 mice with dietary obesity and diabetes. UCP1 expression levels were similar to those obtained by injection into Epi (data not shown). Food intake was significantly decreased by UCP1 expression, as compared with LacZ expression, in subcutaneous fat (Figure 3A), but the effects were much smaller than those produced by UCP1 expression in Epi (Figure 2C). Furthermore, there were no statistically significant decreases in blood glucose (Figure 3B), insulin (Figure 3C), or leptin (Figure 3D) levels. Thus, exogenous UCP1 expression in subcutaneous fat was far less effective in improving insulin and leptin resistance than that in intra-abdominal fat tissue. These findings suggest the anatomical location of the manipulated adipose tissue to be involved in the observed therapeutic effects, which would appear to be important for understanding the metabolic differences between visceral fat-dominant and subcutaneous fat-dominant obesity.

How does the signal (or signals) from intra-abdominal fat tissue exert these remote effects? The importance of anatomical fat-tissue location suggests the involvement of neuronal signaling. The afferent activity from Epi is reportedly transmitted through the nerve bundle, which runs alongside blood vessels supplying Epi, in rats (Niijima, 1998). To study the possible involvement of neuronal signals from Epi, we dissected this nerve bundle in mice with dietary obesity and diabetes. Ten days after bilateral nerve-bundle dissection, adenoviruses were injected into Epi. No significant differences in body weights or Epi weights were observed between sham-operated and nerve-dissected mice (data not shown). While UCP1 adenoviral administration significantly decreased food intake in sham-operated mice, nerve dissection blunted this decrease in food intake such that it was no longer statistically significant (Figure 3E). Similarly, nerve dissection blunted a decrease in hypothalamic NPY mRNA expression, rendering it statistically insignificant (NPY; LacZ versus UCP1: 12.06 ± 6.16 versus 6.39 ± 3.10; $p = 0.15$). These findings suggest that neuronal signals from intra-abdominal fat tissue are involved in food-intake regulation. In contrast, in nerve-dissected mice, blood glucose (Figure 3F) as well as serum insulin (Figure 3G) and leptin (Figure 3H) levels were significantly suppressed in a fashion similar to in sham-operated mice. Thus, improved insulin resistance is largely independent of this neuronal pathway.

To confirm that afferent-nerve signals are involved in UCP1-expression-mediated suppression of food intake, we next examined the effects of functional deafferentation by administering capsaicin (Fu et al., 2003), a selective neurotoxin for unmyelinated C fibers. In LacZ mice, food intake was not altered by capsaicin treatment 10 days prior to adenoviral administration. In contrast, capsaicin pretreatment significantly reversed the food-intake suppression induced by UCP1 expression in Epi (Figure 3I). The inhibitory effect of capsaicin pretreatment was very similar to that of local-nerve dissection (Figure 3E). Taken together, these observations suggest that afferent-nerve signals from Epi are involved in food-intake regulation. To elucidate the molecular mechanism whereby UCP1 expression in Epi modulates neuronal activity, we searched for genes upregulated by adipose UCP1 expression. Using the DNA microarray technique, gene expressions were examined in LacZ- and UCP1-adenovirus-treated Epi (Table S1) and in 3T3-L1 adipocytes (Table S2). With the exception of UCP1, however, there was no overlap in genes showing significantly increased expression. Although further expression profiling including proteomic approaches might elucidate the underlying mechanisms, the apparent lack of genes showing increased expression raises the possibility that the activation of afferent nerves does not involve gene-expression alterations. For instance, UCP1 generates heat, and a capsaicin receptor, TRPV1, is activated by a slightly above normal body temperature (Caterina et al., 1997). Capsaicin treatment affected UCP1-induced food-intake suppression (Figure 3I), raising the possibility that UCP1 expression activates capsaicin-sensitive nerves via TRPV1 activation. Another possibility is involvement of reactive oxygen species, which are affected by mitochondrial uncoupling (Bernal-Mizrachi et al., 2005; Jezek et al., 2004) and reportedly regulate capsaicin-sensitive afferent fibers (Ruan et al., 2005). Further studies are required to examine these hypotheses.

In this study, very limited UCP1 expression in Epi markedly improved insulin and leptin resistance, thereby improving glucose tolerance and decreasing food intake. UCP1 mice were more insulin sensitive than pair-fed LacZ mice. In addition, in db/db mice, despite no food-intake suppression, blood glucose

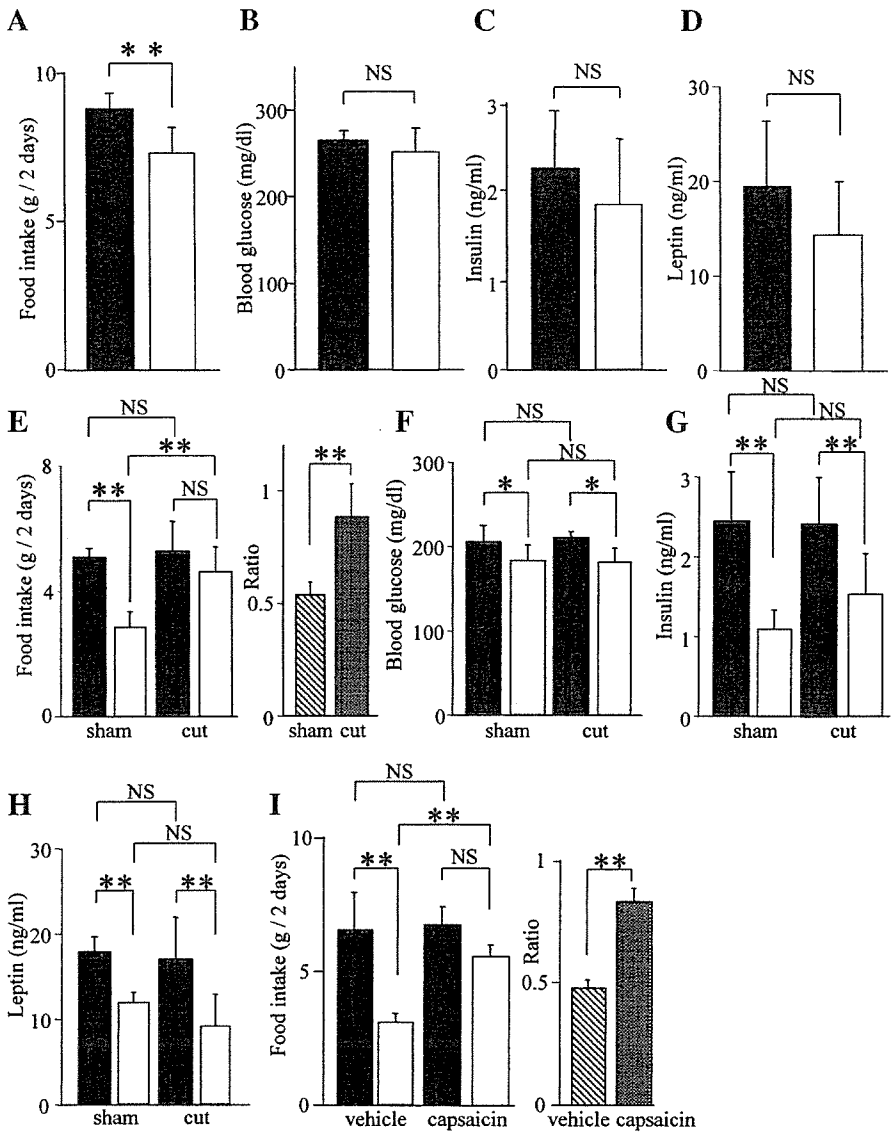

Figure 3. Neuronal signals are likely to be involved in food-intake regulation

A–D) LacZ (black bars) or UCP1 (white bars) adenovirus was injected into subcutaneous fat, and metabolic markers were measured. Total food intakes on days 2 and 3 after adenoviral administration are presented. Blood glucose (**B**), insulin (**C**), and leptin (**D**) levels were determined after a 10 hr fast on day 3 after adenoviral administration. **p < 0.01 by unpaired t test.

E–H) Mice were subjected to local-nerve dissection 10 days prior to adenoviral injection into Epi. Total food intakes of sham-operated (sham) and nerve-dissected (cut) mice (**E**) on days 2 and 3 are presented graphically. Blood glucose (**F**), serum insulin (**G**), and leptin (**H**) levels were determined on day 3.

I) Mice were treated with capsaicin or vehicle 10 days prior to adenoviral injection into Epi. Total food intakes on days 2 and 3 after administration of LacZ (black bars) or UCP1 (white bars) adenovirus are presented. In (**E**) and (**I**), the food intakes of UCP1 mice are expressed in the right graph as ratios to those of LacZ mice. **p < 0.01 assessed by one-factor ANOVA. Data are presented as means ± SD.

and insulin levels were modestly but significantly decreased by UCP1 expression in Epi. Thus, the mechanism underlying improved insulin sensitivity with UCP1 expression in Epi is, in part, independent of leptin signaling and food-intake suppression (Figure 4). Dissection of the nerve bundle from Epi did not alter the decreases in blood glucose and insulin levels. Taken together with the findings that UCP1 expression in subcutaneous fat did not significantly decrease blood glucose or insulin levels, our observations indicate that nonneuronal signals including humoral factors from intra-abdominal adipose tissue possibly participate in systemic improvement of insulin resistance. Since UCP1 expression was observed in a very limited population of adipocytes in Epi, suppression of insulin-resistant adipocytokine secretion is unlikely to explain the beneficial effects. Serum adiponectin levels were not altered, suggesting involvement of other unknown insulin-sensitizing factor (or factors).

On the other hand, decreased food intake is likely to be, at least partially, mediated by afferent-nerve signals from Epi (Figure 4). Afferent-nerve signals from Epi to the central nervous system reportedly result in a reflex from epididymal fat to white adipose tissues via efferent sympathetic-nerve activation (Niijima, 1998; Tanida et al., 2000). In addition, vagal afferent

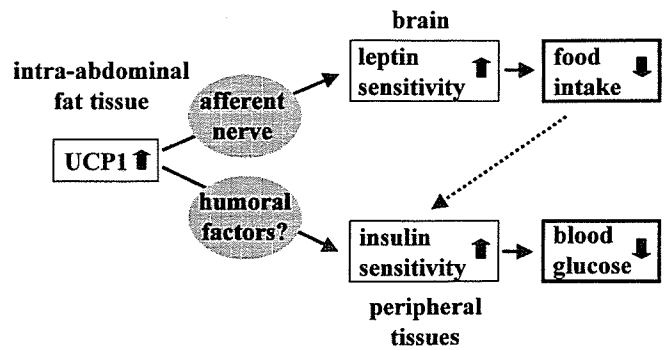

Figure 4. The proposed mechanism whereby UCP1 expression in Epi decreases food intake and improves glucose tolerance

neuronal signals from intra-abdominal tissues, including the gut (Fu et al., 2003; Smith et al., 1981) and the liver (Friedman, 1998; Scharrer, 1999), are known to play a part in regulating food intake. We also reported that UCP1 gene administration into the liver modulates food intake (Ishigaki et al., 2005). Herein we report that intra-abdominal fat tissue is likely to convey metabolic signals to the brain via a neuronal pathway, in addition to via the circulation, resulting in modulation of food intake. Although the precise molecular mechanism remains to be elucidated, this neuronal pathway might play a role in development of the metabolic syndrome, making it a potentially novel therapeutic target.

Experimental procedures

Preparation of recombinant adenovirus

Recombinant adenovirus containing murine UCP1 cDNA (Ishigaki et al., 2005) was constructed as described previously (Katagiri et al., 1996). Recombinant adenoviruses bearing the bacterial β-galactosidase gene (*Adex1CAlacZ*) and green fluorescent protein (AdCMV-GFP) were used as controls.

Animals and in vivo adenovirus injection into fat pad

Animal studies were conducted in accordance with the institutional guidelines for animal experiments at Tohoku University. Male C57BL/6N and AKR/N mice were housed individually, and high-fat-chow feeding (32% safflower oil, 33.1% casein, 17.6% sucrose, and 5.6% cellulose) (Ishigaki et al., 2005) was initiated at 5 weeks of age. After 4 weeks of high-fat-chow loading, body-weight-matched mice were anesthetized prior to dissection of the skin and body wall. The adenoviral preparation (1×10^8 plaque-forming units in a volume of 20 μl) was injected at two points each on each side of the epididymal fat pad or subcutaneous fat tissues in the flank, i.e., a total of four points. KK mice and KK-Ay mice maintained on a standard diet (65% carbohydrate, 4% fat, 24% protein) were similarly administered adenoviruses at 9 weeks and 5 weeks of age, respectively.

Immunoblotting

Tissue protein extracts (250 μg total protein) were boiled in Laemmli buffer containing 10 mM dithiothreitol, subjected to SDS-polyacrylamide gel electrophoresis, and transferred onto nitrocellulose filters. The filters were incubated with anti-UCP1 antibody (Santa Cruz Biotechnology, Santa Cruz, California) and then with anti-goat immunoglobulin G coupled to horseradish peroxidase. The immunoblots were visualized with an enhanced chemiluminescence detection kit (Amersham, Buckinghamshire, UK). The intensities of bands were quantified with the NIH Image 1.62 program.

Histological analysis

Mouse epididymal fat and BAT were immunostained as previously reported (Ishigaki et al., 2005). Mature white adipocytes were identified by their characteristic unilocular appearance. Diameters of 100 or more white adipocytes per mouse in each group were traced manually and analyzed.

Oxygen consumption

Oxygen consumption was measured as previously reported (Ishigaki et al., 2005).

Pair-feeding experiments

Pair-feeding experiments were performed as previously described (Ishigaki et al., 2005).

Blood analysis

Blood glucose and serum insulin, leptin, adiponectin, TNFα, total cholesterol, triglyceride, and free-fatty-acid levels were determined as previously described (Ishigaki et al., 2005).

Measurement of quantitative RT-PCR-based gene expression

The skull was reflected from the brain and the hypothalamus was isolated by snap freezing in liquid nitrogen as previously reported (Bjorbaek et al., 1998). Total RNA was isolated from mouse hypothalamus, fat tissues, or 3T3-L1 adipocytes with ISOGEN (Wako Pure Chemical Co., Osaka, Japan), and cDNA synthesized from total RNA was evaluated with a real-time PCR quantitative system (Light Cycler Quick System 350S; Roche Diagnostics GmbH, Mannheim, Germany).The relative amount of mRNA was calculated with β-actin mRNA as the invariant control. The primers used are shown in Table S3.

Glucose-, insulin-, and leptin-tolerance tests

Glucose-tolerance tests were performed on fasted (10 hr, daytime) mice. Mice were given glucose (2 g/kg of body weight) intraperitoneally, followed by measurement of blood glucose levels. Insulin-tolerance tests were performed on ad libitum-fed mice. Mice were intraperitoneally injected with human regular insulin (0.75 U/kg of body weight; Eli Lilly Co., Kobe, Japan).

Leptin-tolerance tests were carried out as described in a previous report (Igel et al., 1997), with slight modification. Fasted (12 hr) mice were injected with mouse leptin (7.2 mg/kg of body weight; R&D Systems, Inc.) intraperitoneally, and food intakes were monitored for 12 hr after the injection. To examine effects on body-weight change, these two groups of mice were given leptin daily starting on the day of adenoviral administration. Each mouse was then weighed.

Capsaicin treatments

Capsaicin treatment was performed as described in a previous report (Fu et al., 2003), with minor modification. Mice were anesthetized prior to subcutaneous injection of capsaicin solution (50 mg/kg, 12.5 mg/ml dissolved in vehicle). The control group received vehicle treatment (10% Tween 80, 10% ethanol, and 80% saline) under identical administration conditions. Adenoviral administration into Epi was carried out 10 days later.

Local-nerve dissection

The small nerve bundle which runs along side blood vessels supplying Epi was dissected as previously reported (Niijima, 1998). Ten days after bilateral dissection of this nerve bundle, adenoviruses were injected into epididymal fat pad.

Measurement of ATP

Fully differentiated 3T3-L1 adipocytes were infected with recombinant adenoviruses as previously described (Katagiri et al., 1996). Intracellular ATP levels were measured using an ATP determination kit (TOYO B-Net, Tokyo, Japan).

Microarray experiments

Total RNA from epididymal fat or 3T3-L1 adipocytes was used to synthesize cRNA, which was then hybridized to an HG-U133A oligonucleotide array (Affymetrix, Santa Clara, California) according to standard protocols, as described previously (Hippo et al., 2002).

Statistical analysis

All data were expressed as means ± SD. The statistical significance of differences was assessed by the unpaired t test and one-factor ANOVA.

Supplemental data

Supplemental Data include four figures and three tables and can be found with this article online at http://www.cellmetabolism.org/cgi/content/full/3/3/223/DC1/.

Acknowledgments

We appreciate Drs. L.P. Kozak (Pennington Biomedical Research Center) and H. Mizuguchi (National Institute of Biomedical Innovation) for the generous gifts of UCP1 cDNA and GFP-adenovirus, respectively. We thank Ms. H. Meguro (Tokyo University) for technical support. This work was supported by a Grant-in-Aid for Scientific Research (B2, 15390282) and a Grant-in-Aid for Exploratory Research (15659214) to H.K. from the Ministry of Education, Science, Sports and Culture of Japan and a Grant-in-Aid for Scientific Research (H16-genome-003) to Y.O. from the Ministry of Health, Labor and Welfare of Japan. This work was also supported by the 21st Century COE Programs "CRESCENDO" (H.K.) and "the Center for Innovative Therapeutic Development for Common Diseases" (Y.O.) of the Ministry of Education, Science, Sports and Culture.

Received: June 22, 2005
Revised: October 12, 2005
Accepted: February 1, 2006
Published: March 7, 2006

References

Bernal-Mizrachi, C., Gates, A.C., Weng, S., Imamura, T., Knutsen, R.H., DeSantis, P., Coleman, T., Townsend, R.R., Muglia, L.J., and Semenkovich, C.F. (2005). Vascular respiratory uncoupling increases blood pressure and atherosclerosis. Nature *435*, 502–506.

Bjorbaek, C., Elmquist, J.K., Frantz, J.D., Shoelson, S.E., and Flier, J.S. (1998). Identification of SOCS-3 as a potential mediator of central leptin resistance. Mol. Cell *1*, 619–625.

Bjorntorp, P. (1992). Abdominal fat distribution and disease: an overview of epidemiological data. Ann. Med. *24*, 15–18.

Caterina, M.J., Schumacher, M.A., Tominaga, M., Rosen, T.A., Levine, J.D., and Julius, D. (1997). The capsaicin receptor: a heat-activated ion channel in the pain pathway. Nature *389*, 816–824.

Cederberg, A., Gronning, L.M., Ahren, B., Tasken, K., Carlsson, P., and Enerback, S. (2001). FOXC2 is a winged helix gene that counteracts obesity, hypertriglyceridemia, and diet-induced insulin resistance. Cell *106*, 563–573.

Considine, R.V., Sinha, M.K., Heiman, M.L., Kriauciunas, A., Stephens, T.W., Nyce, M.R., Ohannesian, J.P., Marco, C.C., McKee, L.J., Bauer, T.L., et al. (1996). Serum immunoreactive-leptin concentrations in normal-weight and obese humans. N. Engl. J. Med. *334*, 292–295.

Flier, J.S. (2004). Obesity wars: molecular progress confronts an expanding epidemic. Cell *116*, 337–350.

Friedman, J.M. (2003). A war on obesity, not the obese. Science *299*, 856–858.

Friedman, J.M., and Halaas, J.L. (1998). Leptin and the regulation of body weight in mammals. Nature *395*, 763–770.

Friedman, M.I. (1998). Fuel partitioning and food intake. Am. J. Clin. Nutr. *67*, 513S–518S.

Fu, J., Gaetani, S., Oveisi, F., Lo Verme, J., Serrano, A., Rodriguez De Fonseca, F., Rosengarth, A., Luecke, H., Di Giacomo, B., Tarzia, G., and Piomelli, D. (2003). Oleylethanolamide regulates feeding and body weight through activation of the nuclear receptor PPAR-alpha. Nature *425*, 90–93.

Heymsfield, S.B., Greenberg, A.S., Fujioka, K., Dixon, R.M., Kushner, R., Hunt, T., Lubina, J.A., Patane, J., Self, B., Hunt, P., and McCamish, M. (1999). Recombinant leptin for weight loss in obese and lean adults: a randomized, controlled, dose-escalation trial. JAMA *282*, 1568–1575.

Hippo, Y., Taniguchi, H., Tsutsumi, S., Machida, N., Chong, J.M., Fukayama, M., Kodama, T., and Aburatani, H. (2002). Global gene expression analysis of gastric cancer by oligonucleotide microarrays. Cancer Res. *62*, 233–240.

Igel, M., Becker, W., Herberg, L., and Joost, H.G. (1997). Hyperleptinemia, leptin resistance, and polymorphic leptin receptor in the New Zealand obese mouse. Endocrinology *138*, 4234–4239.

Ishigaki, Y., Katagiri, H., Yamada, T., Ogihara, T., Imai, J., Uno, K., Hasegawa, Y., Gao, J., Ishihara, H., Shimosegawa, T., et al. (2005). Dissipating excess energy stored in the liver is a potential treatment strategy for diabetes associated with obesity. Diabetes *54*, 322–332.

Jezek, P., Zackova, M., Ruzicka, M., Skobisova, E., and Jaburek, M. (2004). Mitochondrial uncoupling proteins—facts and fantasies. Physiol. Res. *53* Suppl. 1, S199–S211.

Katagiri, H., Asano, T., Ishihara, H., Inukai, K., Shibasaki, Y., Kikuchi, M., Yazaki, Y., and Oka, Y. (1996). Overexpression of catalytic subunit p110alpha of phosphatidylinositol 3-kinase increases glucose transport activity with translocation of glucose transporters in 3T3-L1 adipocytes. J. Biol. Chem. *271*, 16987–16990.

Klingenberg, M., and Huang, S.G. (1999). Structure and function of the uncoupling protein from brown adipose tissue. Biochim. Biophys. Acta *1415*, 271–296.

Kopecky, J., Clarke, G., Enerback, S., Spiegelman, B., and Kozak, L.P. (1995). Expression of the mitochondrial uncoupling protein gene from the aP2 gene promoter prevents genetic obesity. J. Clin. Invest. *96*, 2914–2923.

Leonardsson, G., Steel, J.H., Christian, M., Pocock, V., Milligan, S., Bell, J., So, P.W., Medina-Gomez, G., Vidal-Puig, A., White, R., and Parker, M.G. (2004). Nuclear receptor corepressor RIP140 regulates fat accumulation. Proc. Natl. Acad. Sci. USA *101*, 8437–8442.

Matsuzawa, Y., Shimomura, I., Nakamura, T., Keno, Y., and Tokunaga, K. (1995). Pathophysiology and pathogenesis of visceral fat obesity. Ann. N Y Acad. Sci. *748*, 399–406.

Niijima, A. (1998). Afferent signals from leptin sensors in the white adipose tissue of the epididymis, and their reflex effect in the rat. J. Auton. Nerv. Syst. *73*, 19–25.

Ruan, T., Lin, Y.S., Lin, K.S., and Kou, Y.R. (2005). Sensory transduction of pulmonary reactive oxygen species by capsaicin-sensitive vagal lung afferent fibres in rats. J. Physiol. *565*, 563–578.

Scharrer, E. (1999). Control of food intake by fatty acid oxidation and ketogenesis. Nutrition *15*, 704–714.

Smith, G.P., Jerome, C., Cushin, B.J., Eterno, R., and Simansky, K.J. (1981). Abdominal vagotomy blocks the satiety effect of cholecystokinin in the rat. Science *213*, 1036–1037.

Tanida, M., Iwashita, S., Ootsuka, Y., Terui, N., and Suzuki, M. (2000). Leptin injection into white adipose tissue elevates renal sympathetic nerve activity dose-dependently through the afferent nerves pathway in rats. Neurosci. Lett. *293*, 107–110.

Tsukiyama-Kohara, K., Poulin, F., Kohara, M., DeMaria, C.T., Cheng, A., Wu, Z., Gingras, A.C., Katsume, A., Elchebly, M., Spiegelman, B.M., et al. (2001). Adipose tissue reduction in mice lacking the translational inhibitor 4E-BP1. Nat. Med. *7*, 1128–1132.

Um, S.H., Frigerio, F., Watanabe, M., Picard, F., Joaquin, M., Sticker, M., Fumagalli, S., Allegrini, P.R., Kozma, S.C., Auwerx, J., and Thomas, G. (2004). Absence of S6K1 protects against age- and diet-induced obesity while enhancing insulin sensitivity. Nature *431*, 200–205.

ELSEVIER

Mechanisms of Development 123 (2006) 472–480

www.elsevier.com/locate/modo

Evidence for activation of *Amh* gene expression by steroidogenic factor 1

Shuji Takada [a,*], Tomoaki Wada [a], Ruri Kaneda [a,b], Young Lim Choi [a], Yoshihiro Yamashita [a], Hiroyuki Mano [a,b]

[a] *Division of Functional Genomics, Jichi Medical University, 3311-1 Yakushiji, Shimotsuke, Tochigi 329-0498, Japan*
[b] *CREST, Japan Science and Technology Agency, Saitama 332-0012, Japan*

Received 4 March 2006; received in revised form 31 March 2006; accepted 6 April 2006
Available online 5 May 2006

Abstract

The *anti-Müllerian hormone* gene (*Amh*) is responsible for regression in males of the Müllerian ducts. The molecular mechanism of regulation of chicken *Amh* expression is poorly understood. To investigate the regulation of chicken *Amh* expression, we have cloned *Amh* cDNAs from quail and duck as well as the promoter regions of the gene from chicken, quail, and duck. The expression patterns of *Amh* during embryonic development in these three species were found to be similar, suggesting that the regulatory mechanisms of *Amh* expression are conserved. The sequence of the proximal promoter of *Amh* contains a putative binding site for steroidogenic factor 1 (SF1), the protein product of which can up-regulate *Amh* in mammals. We showed here that SF1 is able to activate the chicken *Amh* promoter and binds to its putative SF1 binding site. These results suggest that SF1 plays a role in regulation of *Amh* expression in avian species.

Keywords: *Anti-Müllerian hormone*; Steroidogenic factor 1; Quail; Duck; Chicken; Sex determination; Gonadogenesis

1. Introduction

In birds, the heterogametic pairing of sex chromosomes (ZW) results in female development, whereas males are the heterogametic sex (XY) in mammals. It remains unclear whether avian sex is determined by a master female-determining gene (or genes) on the W chromosome, by Z chromosome gene dosage, or by a combination of both mechanisms (Clinton, 1998). Although the systems for sex determination and differentiation differ between mammals and birds, several genes that are associated with sex differentiation in mammals are expressed in similar patterns in mouse and chicken gonads during development, suggesting that the molecular mechanisms of sexual differentiation are similar to some extent in the two species.

One such gene is that for *anti-Müllerian hormone* (*Amh*), also known as *Müllerian inhibiting substance*, which is expressed from early stages of sexual differentiation, predominantly in pre-Sertoli cells of male embryonic gonads, in mice and chickens (Münsterberg and Lovell-Badge, 1991; Oréal et al., 1998). The product of this gene, AMH, is a member of the transforming growth factor-ß (TGF-ß) superfamily of secreted signaling molecules and induces regression of the Müllerian ducts, the anlagen of the female reproductive tract including the uterus, oviducts, upper vagina, and fallopian tubes (Josso et al., 2001). However, there is a difference between mouse and chicken in the expression patterns of *Amh* that are evident before the appearance of structural differences between the sexes. At this stage, *Amh* is expressed at similar levels in male and female gonads of chicken (Oréal et al., 1998) but is not expressed in mice (Münsterberg and Lovell-Badge, 1991).

The sex and temporal specificities of its expression during embryonic development indicate that *Amh* is a highly regulated gene. The molecular mechanisms of *Amh* expression have been extensively analyzed in mammals, but they are not well characterized in chicken. Analysis of the mammalian *Amh* promoter has revealed that the transcription factors SOX9 and steroidogenic factor 1 (SF1, also known as AD4BP) play central roles in male-specific up-regulation of mouse *Amh*. Targeted mutagenesis of the SOX binding site at nucleotide position −142 in the proximal promoter of mouse *Amh* prevented the initiation of gene transcription (Arango et al., 1999), indicating that SOX9 is essential for the induction of *Amh* expression. In vitro transfection experiments with

* Corresponding author. Tel.: +81 285 58 7449; fax: +81 285 44 7322.
E-mail address: stakada@jichi.ac.jp (S. Takada).

0925-4773/$ - see front matter © 2006 Elsevier Ireland Ltd. All rights reserved.
doi:10.1016/j.mod.2006.04.004

a minimal *Amh* promoter (180 bp) revealed that mutation of the SF1 binding site at position −90 resulted in a marked decrease in transcriptional activity (Shen et al., 1994). Introduction of the same mutation into transgenic mice led to only a slight decrease in *Amh* expression (Arango et al., 1999). This discrepancy may be explained by the existence of another functional SF1 binding site at position −218 (Watanabe et al., 2000).

Characterization of the chicken *Amh* promoter (Oréal et al., 1998) revealed little sequence similarity to that of mouse *Amh*, although two putative SOX binding sites and a putative SF1 binding site were detected. Whether these predicted binding sites are functional has remained unknown, but analysis of the expression of chicken *Sox9* and *Sf1* suggests that the products of these genes are not essential for male-specific up-regulation of chicken *Amh*. *Sox9* is expressed predominantly in developing male gonads during sexual differentiation in the chicken; however, in contrast to the mouse, up-regulation of *Amh* precedes that of *Sox9* (Oréal et al., 2002; Smith et al., 1999a; Takada et al., 2005). Chicken *Sf1* is expressed at similar levels in male and female gonads before sexual differentiation, as is chicken *Amh*; however, after the onset of sexual differentiation, *Sf1* is expressed at a higher level in female gonads than in male gonads, suggesting that SF1 is not responsible for the male-specific up-regulation of *Amh*.

Interaction of the *Amh* promoter with its regulatory factors has not been demonstrated in the chicken. To investigate the molecular mechanism of regulation of *Amh* expression in chicken, we have compared the promoter sequences of three avian species: chicken, quail, and duck.

2. Results

2.1. Cloning and expression patterns of quail and duck Amh

To clone the promoter regions of quail and duck *Amh*, we first attempted to clone quail and duck *Amh* cDNAs by 5′ and 3′ RACE. Primers for RACE were designed on the basis of the sequences of partial genomic fragments of quail and duck *Amh* amplified by PCR with the primers cAmh-4 and TAMHF3, which, in turn, had previously been designed on the basis of the chicken *Amh* cDNA sequence (Western et al., 1999) and used to clone *Amh* cDNA from the red-eared slider turtle, *Trachemys scripta* (Takada et al., 2004). These primers, which are located in the 3′ terminal region of the open reading frame of chicken *Amh*, yielded 391-bp products from the quail and duck genomes (data not shown). Comparison of the DNA sequences of these products with that of chicken *Amh* cDNA (GenBank accession no. X89248) revealed a 27-bp conserved sequence with no mismatches. Sense and antisense oligonucleotides corresponding to this 27-bp sequence were synthesized and used for 3′ and 5′ RACE, respectively. Given that sex differentiation occurs before day 5 in quail embryos and day 7 in duck embryos (Takada et al., 2006), we used RNA purified from the gonads of male quail and duck embryos on days 7 and 8, respectively, as a template for RACE. The nucleotide sequences of 5′ and 3′ RACE products were determined and assembled to yield the corresponding cDNA sequences.

To verify the authenticity of the sequences determined by 5′ and 3′ RACE for each species, we attempted to amplify cDNAs containing the entire coding regions of quail and duck *Amh* by RT-PCR with primers that map to the corresponding 5′ and 3′ untranslated regions. A 2.0-kb cDNA was amplified from RNA prepared from quail or duck. Nucleotide sequencing of each of the amplified fragments confirmed that the 5′ and 3′ RACE sequences were linked in tandem for both quail and duck, demonstrating that the assembled sequences correspond to single transcripts.

The putative proteins encoded by the quail and duck cDNAs comprise 644 and 670 amino acids, respectively. A search for protein motifs with CD-Search (Marchler-Bauer and Bryant, 2004) revealed that both deduced amino acid sequences contain the 99-residue TGF-ß motif at their COOH-termini, with 97, 94, and 94 residues of this motif being identical in the quail protein and chicken AMH, in the duck protein and chicken AMH, and in the quail and duck proteins, respectively, (Fig. 1). The overall sequence identities of the three avian proteins are 94.0, 76.5, and 75.3% for quail and chicken, duck and chicken, and quail and duck, respectively, despite the previous finding that the amino acid sequence of AMH is poorly conserved among vertebrates (Carré-Eusèbe et al., 1996; Neeper et al., 1996; Western et al., 1999). Given that a BLASTP search of the non-redundant GenBank database with the deduced amino acid sequences of the quail and duck proteins as queries yielded *Gallus gallus* (chicken) AMH followed by *Macropus eugenii* (wallaby) AMH and *Alligator mississippiensis* (American alligator) AMH as the most similar sequences, we conclude that the isolated quail and duck cDNAs are derived from the corresponding *Amh* genes. The nucleotide sequences of these quail and duck cDNAs have been deposited in GenBank under the accession numbers AY904049 and AY904047, respectively.

We next examined the spatiotemporal expression patterns of quail and duck *Amh* during the early stages of gonadal differentiation with the use of whole-mount in situ hybridization. Gonad–mesonephros complexes were isolated from quail embryos on days 4, 5, 6, and 7 (Zacchei stages 17 to 18, 20 to 21, 22, and 24, respectively), (Zacchei, 1961) and from duck embryos on days 6, 7, 8, and 9. Duck embryos were staged by comparison with chicken (Hamburger and Hamilton, 1951). The morphological stages of duck are essentially the same as those of chicken, although development is slightly delayed in duck embryos (days 6, 7, 8, and 9 for duck embryos correspond to Hamburger and Hamilton stages 25 to 26, 28, 29 to 30, and 31 to 32, respectively). *Amh* mRNA was not detected in quail gonads on day 4 (Fig. 2A,F) or in duck gonads on day 6 (Fig. 2J,O). *Amh* expression was observed in male and female gonads both of quail on days 5, 6, and 7 (Fig. 2B–D,G–I) and of duck on days 7, 8, and 9 (Fig. 2K–M,P–R), with expression levels being higher in male than in female. Sense control probes yielded no specific labeling (Fig. 2E,N). The earliest

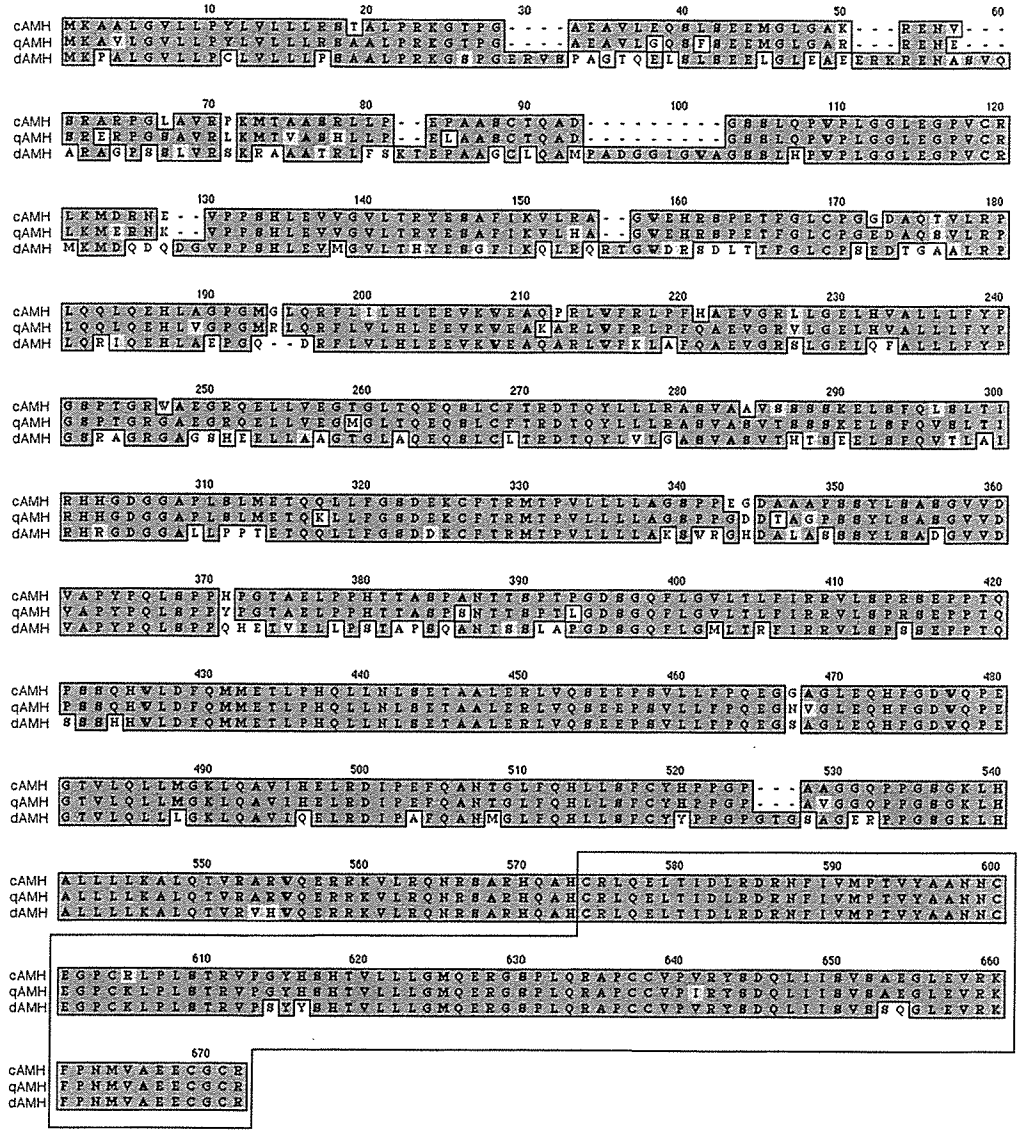

Fig. 1. Alignment of the deduced amino acid sequences of chicken (c), quail (q), and duck (d) AMH. Dark and light gray shading indicate identical and similar amino acids, respectively. The boxed region corresponds to the TGF- ß motif.

detectable stages for male-specific up-regulation of *Amh* were thus similar for chicken (stages 28–30) (Loffler et al., 2003; Morais da Silva et al., 1996; Oréal et al., 1998; Smith et al., 1999a), quail (day 5, corresponding to Zacchei stages 20 to 21 and Hamburger and Hamilton stages 27–29) (Zacchei, 1961), and duck (day 7, corresponding to Hamburger and Hamilton stage 28). These similar expression patterns suggest that regulation of *Amh* expression is conserved among these three avian species. The expression patterns of quail and duck *Amh* are also similar to those of quail and duck *Sox9* (Takada et al., 2006). The earliest detectable stages examined so far for male-specific up-regulation of *Amh* and *Sox9* is same in quail and duck (quail at day 5and duck at day 7), however, there was a difference in expression patterns between *Amh* and *Sox9* in female gonads of quail and duck; *Amh* is expressed at low levels but *Sox9* is not.

2.2. Cloning and nucleotide sequence analysis of chicken, quail, and duck Amh promoters

To isolate the promoters of chicken, quail, and duck *Amh*, we used PCR with primers based on the sequences of *Amh* and of a gene located upstream of *Amh* in the avian genome. BLAT analysis (February 2004 assembly, http://genome.ucsc.edu/cgi-bin/hgBlat, International Chicken Genome Sequencing Consortium, 2004) with the chicken *Amh* sequence as a query identified *Sap62* (also known as *Sf3a2*) as being located upstream of and adjacent to *Amh*. Primers were thus designed on the basis of open reading frame sequences conserved between chicken (NM_001004397) and mouse (NM_013651) *Sap62* and among chicken (X89248), quail, and duck *Amh*. These primers yielded 5328- and 4651-bp products from the chicken and quail genomes, respectively,

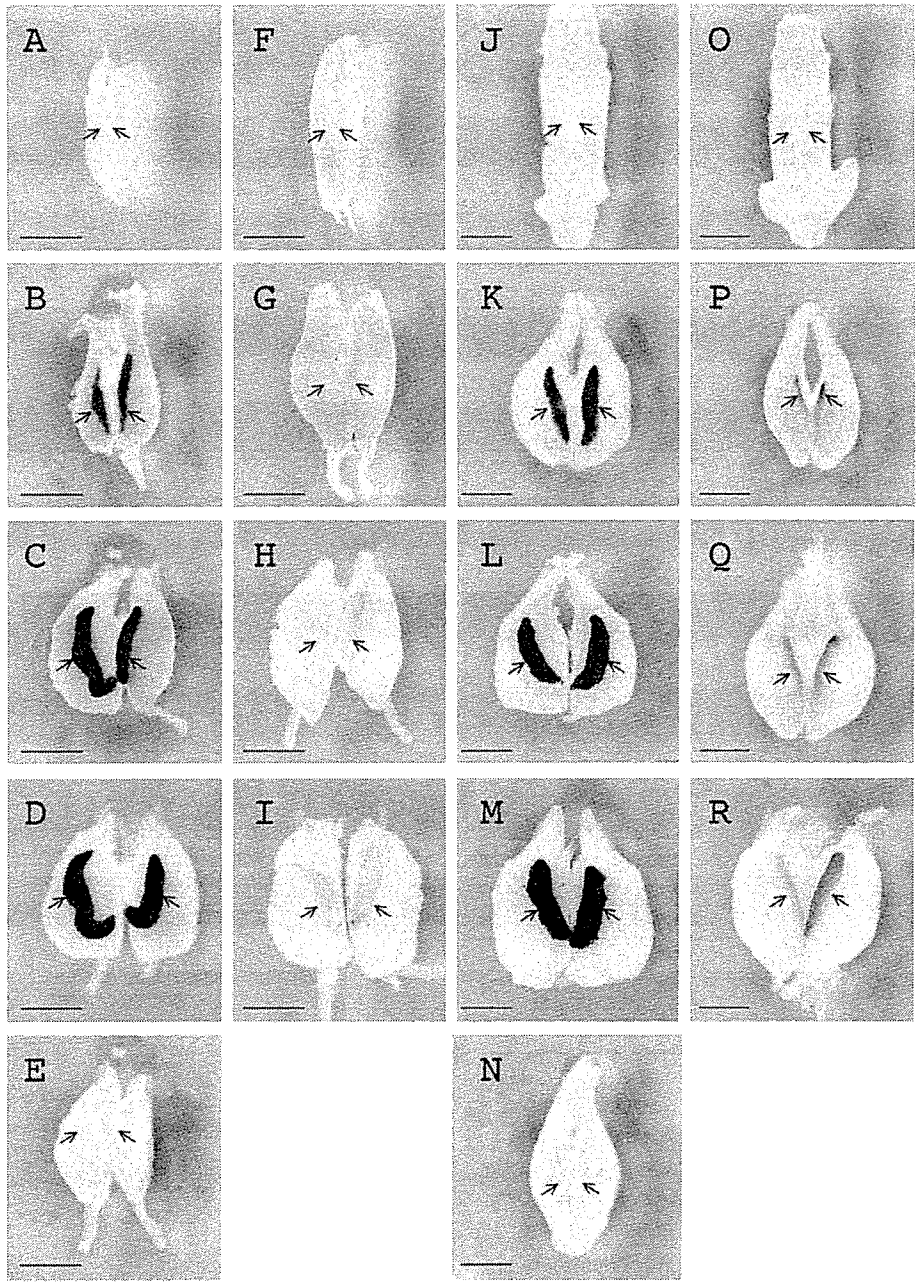

Fig. 2. Whole-mount in situ hybridization analysis of *Amh* expression in the embryonic gonad–mesonephros of quail and duck. Male (A–E) and female (F–I) quail embryos were analyzed on day 4 (A, F) day 5 (B, G), day 6 (C, E, H), and day 7 (D, I). Male (J–N) and female (O–R) duck embryos were analyzed on day 6 (J, O) day 7 (K, P, N), day 8 (L, Q), and day 9 (M, R). All embryos were subjected to hybridization with an antisense probe, with the exception of those in (E) and (N), for which a sense probe was used as a control. Arrows indicate the positions of the gonads. Scale bars, 1 mm.

but no product was obtained from the duck genome. The chicken and quail products were sequenced and the resulting sequences were used to design a primer for amplification of the duck *Amh* promoter. A 5793-bp PCR product was thus obtained from the duck genome. Sequence analysis revealed that the orientations of *Sap62* and *Amh* are the same in all three avian species. The nucleotide sequences of these genomic fragments (excluding the primer sequences) have been deposited in GenBank under the accession numbers DQ269189 for chicken, DQ269190 for quail, and DQ269191 for duck.

The similarity in the expression patterns of *Amh* among chicken, quail, and duck embryos suggested that the regulatory sequences responsible for the control of *Amh* expression are also conserved among these species. To identify regulatory elements that might mediate up- or down-regulation of *Amh* expression, we first compared the promoter sequences among the three species. The sequences obtained by PCR from chicken and quail spanned from exon 2 of *Sap62* to exon 1 of *Amh*, whereas that obtained from duck spanned from exon 3 of *Sap62* to exon 1 of *Amh*. To compare corresponding